An integrate-and-fire spiking neural network model simulating artificially induced cortical plasticity

Larry Shupe[1], Eberhard E. Fetz[12*]

[1] Department of Physiology and Biophysics, University of Washington, Seattle, Washington, United States of America

[2] Washington National Primate Research Center, University of Washington, Seattle, Washington, United States of America

* Corresponding author

E-mail: fetz@uw.edu (EEF)

Abstract

We describe an integrate-and-fire (IF) spiking neural network that incorporates spike-timing dependent plasticity (STDP) and simulates the experimental outcomes of four different conditioning protocols that produce cortical plasticity. The original conditioning experiments were performed in freely moving non-human primates with an autonomous head-fixed bidirectional brain-computer interface. Three protocols involved closed-loop stimulation triggered from (a) spike activity of single cortical neurons, (b) EMG activity from forearm muscles, and (c) cycles of spontaneous cortical beta activity. A fourth protocol involved open-loop delivery of pairs of stimuli at neighboring cortical sites. The IF network that replicates the experimental results consists of 360 units with simulated membrane potentials produced by synaptic inputs and triggering a spike when reaching threshold. The 240 cortical units produce either excitatory or inhibitory post-synaptic potentials in their target units. In addition to the experimentally observed conditioning effects, the model also allows computation of underlying network behavior not originally documented. Furthermore, the model makes predictions about outcomes from protocols not yet investigated, including spike-triggered inhibition, gamma-triggered stimulation and disynaptic conditioning. The success of the simulations suggests that a simple voltage-based IF model incorporating STDP can capture the essential mechanisms mediating targeted plasticity with closed-loop stimulation.

Author summary

Previous experiments have shown that the connections between neurons in the brain can be modified by several different activity-dependent stimulation methods. Understanding the underlying mechanisms that mediate these changes is key to designing effective protocols for producing targeted plasticity in clinical and basic science applications. We describe a simple but powerful neural network model that replicates a wide range of experimental results. It provides valuable additional information about the underlying processes and more importantly, predicts new protocols that have never been tested but could be. The network model is composed of interconnected "integrate-and-fire" units that, like biological neurons, add the inputs they receive and fire when the results exceed threshold. The model also includes a well-documented rule for changing the strength of connections between two units based on the relative timing of their activity.

The model captures the neural plasticity produced in recent experiments that delivered activity dependent stimulation or controlled patterns of stimulation. The model explores how such paradigms would strengthen indirect as well as direct neural connections. It also predicts that a new experimental protocol using easily recorded neural signals would be very effective in modifying neural connections. The results represent a major advance in understanding fundamental neural mechanisms and designing new protocols for inducing targeted neural plasticity.

Introduction

Computational neural network models provide a powerful tool for understanding mechanisms of neural computation and for exploring network behavior in ways that physiological recordings cannot [1-4]. Neural networks consisting of integrate-and-fire (IF) spiking units have proven useful in studying network dynamics produced by spiking neurons (for reviews see [5-11]). The IF units typically sum inputs to produce a simulated membrane potential function that triggers a spike when it reaches a threshold. The inputs can simulate postsynaptic potentials with rise time and decay; the units can also incorporate biophysical conductances [12]. Spike-timing-dependent plasticity (STDP) rules [13-16] can be incorporated into IF networks to investigate consequent changes in synaptic connections on network dynamics. For example, large networks of biophysically realistic spiking units with STDP have been shown to form functional interacting groups [17-20] and capture global changes induced by conditioning [21]. We here used an IF network with STDP to simulate experimental results from recent physiological conditioning studies performed with a closed-loop brain computer interface (CL-BCI).

The strength of synaptic connections between motor cortical neurons has been experimentally modified by several different conditioning protocols. In non-human primates (NHP), CL-BCIs have induced plasticity with spike-triggered stimulation of neighboring cortical sites during free behavior [22]. After a day of conditioning the output effects on muscles and isometric wrist responses evoked by microstimulation of the recording site (labeled A) included the output effects evoked from the stimulation site (B), consistent with a strengthening of connections from A to B. Changes occurred only for spike-stimulus delays of 50 ms or less, consistent with

61 the time course of STDP. These changes lasted for up to 10 days post-conditioning. A second
62 conditioning paradigm triggered cortical stimulation from pulses generated by
63 electromyographic activity of a forearm muscle [23]. This produced changes in the output
64 effects evoked by stimulating the cortical site (A) that was associated with the recorded muscle
65 to now include effects evoked from the stimulated site (B). Again, the results were consistent
66 with a strengthening of connections from A to B. A third conditioning paradigm used paired
67 sequential stimulation of sites A and B and found changes in the magnitude of potentials at B
68 evoked by stimulation at A [24]. These effects were found at some, but not all site pairs, and
69 were again seen for stimulus intervals of 30 ms or less. A fourth conditioning paradigm
70 produced cortical plasticity using a CL-BCI to stimulate site A during specific phases of
71 spontaneous beta oscillations at B [25]. This produced transient changes in the connection
72 from A to B; the connections increased or decreased, depending on whether stimuli were
73 delivered during the phase in which neurons at B would tend to be depolarized or
74 hyperpolarized, respectively. These changes in connectivity were induced by spontaneous
75 oscillatory episodes with 3 or more cycles and decayed within seconds.

76 We here investigated whether the neural mechanisms underlying these four conditioning
77 protocols could be captured by an IF neural network model that incorporates STDP. This
78 approach differs from a previous neural network model using populations of Poisson firing units
79 to analytically compute the net effects produced by spike-triggered stimulation [26] (See
80 Discussion). Our IF model replicated the results of all four conditioning protocols with a single
81 set of network parameters and enabled derivations beyond the original experimental
82 observations, providing a more complete picture of conditioned changes and insights into the

83 effects of relevant network parameters. Furthermore, the model also provided totally novel
84 predictions about the outcomes of possible conditioning experiments that have not yet been
85 performed. Thus, there is a productive symbiotic relation between the model and physiological
86 experiments. Our IF model provides a powerful tool for elucidating the synaptic mechanisms
87 underlying cortical plasticity and discovering new conditioning paradigms.

88

89 Results

90 The model

91 The IF model consists of 360 integrate-and-fire units with a "membrane potential" that
92 integrates synaptic inputs and upon reaching threshold triggers a spike and resets (Fig 1A; see
93 Methods for more detail). After a conduction delay the spike generates excitatory or inhibitory
94 post-synaptic potentials in connected target units that are proportional to the size of the
95 synaptic weights (Fig 1A and B). During conditioning the synaptic weights are modified by a
96 STDP function that depends on the relative timing of pre- and postsynaptic spikes (Fig 1C).

97 **Fig 1. Integrate and fire model.** (A) External input (Ej) and spiking input from connected
98 units (U1 to Un) are summed into a target unit's potential (Vj). When a unit's potential
99 reaches threshold it is reset to 0 and the unit sends a spike to all its target units. The spike
100 evokes an excitatory or inhibitory post synaptic potential proportional to synaptic weight w_{ij}.
101 (B) PSP Shape is calculated as the difference between two exponential functions (dotted and
102 dashed lines). (C) The Spike Timing-Dependent Plasticity Curve shows how much weight w_{ij} is
103 changed given the difference in spike times between the target unit *i* and the source unit *j*.

The network contains 240 cortical units grouped into three “columns”, A, B and C (Fig 2A). Excitatory and inhibitory units within a column are sparsely interconnected, and excitatory units connect sparsely to units of other columns. Units also receive excitatory external drive consisting of uncorrelated and correlated spike events (Fig 2A and B). Each column also has an associated group of 40 motor units with graded thresholds and EMG potentials (Fig 2B). In addition to spike events the model monitors the “local field potentials” calculated as the sum of all postsynaptic potentials within a column (Fig 2C).

Fig 2. Network connectivity. (A) Cortical network configuration. Units are grouped into 3 columns A, B, and C. Each column contains 40 excitatory units (e.g. Ae1 … Ae40) and 40 local inhibitory units (Ai) all sparsely interconnected. Only excitatory units project to other columns. Columns also receive external input, consisting of correlated and uncorrelated (C/U) exponentially distributed spikes. (B) Column configuration. Associated with each cortical column is a pool of motor units that produce muscle potentials (EMG). The dashed lines designate unmodifiable connections. (C) Example spiking activity of excitatory (e), inhibitory (i) and motor units (m) associated with each column. LFP is the sum of within-column post-synaptic potentials in e and i units.

Electrical stimulation is simulated by a large excitatory input delivered simultaneously to all units of a column. During conditioning stimuli can be triggered by other activity or delivered in open-loop mode. Test stimuli can be delivered to document the magnitude of net excitatory connections between columns by the size of the evoked local field potentials.

124 **Spike-triggered stimulation**

125 To simulate conditioning with spike-triggered stimulation [22,27], each time the first excitatory
126 unit (Ae1) in Column A fired, a conditioning stimulus was applied to all units in Column B at a
127 given delay (Fig 3A). Conditioning effects were observed as increased connection strengths
128 between Column A and Column B. Fig 3C shows color-coded strengths of all connections after
129 spike-triggered stimulation with a spike-stimulus delay of 10 ms, showing strengthened
130 connections from Ae to B units relative to connections between other columns. Connectivity
131 between Columns A and B was also documented by the average evoked potential (EP) (Fig 3D
132 insets) in the LFP of Column B produced by a test stimulus to A (Fig 3A).

133 **Fig 3. Spike-triggered stimulation.** (A) A Conditioning stimulus (ST) is applied to all units in
134 Column B at a delay from each trigger spike (T) detected on the first excitatory unit (Ae1) of
135 Column A. Testing shows stimulus applied to all Column A units to evoke a potential (EP) in
136 LFP of Column B. (B) Histogram of excitatory A and B unit firings aligned with spikes on Ae1
137 (T) during conditioning with a 10 ms delayed stimulus. (C) Final connection strengths
138 (calibrated in uV) between units after conditioning. (D) Average percent increase in the EP as
139 a function of the delay between trigger spike and stimulation. Insets show average EPs
140 before and after conditioning for two delays. Grey dashed line shows the EP response in
141 Column B after tetanic stimulation of Column B.

142 After conditioning for 500 seconds of simulation time, the conditioning unit (Ae1) showed near
143 maximum connection strengths to its target units in Column B. Other units in A also show
144 increased connections to B depending on the percent of correlated bias inputs to A. Networks

145 with 30% correlated bias inputs show a moderate conditioned response in other Column A→B
146 connections. Networks with 20% correlated bias inputs show little conditioned response
147 except for connections from unit Ae1. Fig 3B shows the activity in the entire Ae population
148 aligned with the triggering Ae1 spike times (T). The sharp peak at 0 ms represents the trigger
149 spikes and the broad peri-trigger peak reflects the synchrony between Ae units imposed by 30%
150 external correlated bias. Fig 3B also shows the times of spikes in Column B (red); the large peak
151 at 10 ms reflects the occurrence of stimulus pulses in B.

152 Fig 3D shows the size of A→B EPs after spike-triggered conditioning at various spike-stimulus
153 delays. The peak in the curve reflects the effect of the STDP rule. At long delays, the spike-
154 triggered conditioning effect approaches the small effect of tetanic stimulation applied to
155 Column B (dashed line). At "zero" delay the size of the EP is decreased (Fig 3D). In this case the
156 spike-stimulus delay is shorter than the conduction delay and connections from A to B become
157 weaker. This decrease in synaptic strength is consistent with the STDP rule and with
158 experimental results obtained for corticospinal connections [28].

159 The original experiments of Jackson et al [22] could not document the conditioning effects by
160 recording short-latency EPs because of stimulus artifacts, so instead measured conditioning
161 effects indirectly by using cortical microstimulation to evoke EMG responses. To simulate these
162 experimental observations, the motor unit pools were activated by trains of cortical stimuli
163 delivered at separate times to each column (Fig 4). This simulation shows that after
164 conditioning, stimulation of Column A now also evoked responses in the muscle of Column B,
165 mediated by the strengthened A→B connections and as reported by Jackson et al (their figure
166 2).

167 **Fig 4. Simulation of output effects on muscles before and after spike-triggered stimulation.**
168 Averages of rectified EMG responses evoked by repetitive stimulation of Column A
169 (containing conditioning trigger unit), Column B (stimulus column), and Column C (control) for
170 preconditioning (blue) and post-conditioning (orange) periods (cf. figure 2 in [22]). For this
171 simulation, inter-column connection probability was doubled to 1/3 and the correlated bias
172 drive was set to 50%. The test stimulus train was 1 mV, 25 pulses, 500 Hz delivered during
173 intervals marked by black bars (the response delay is due to the 10 ms corticospinal
174 conduction time). Ordinate scale is in millivolts.

175 **EMG-triggered stimulation**

176 Cortical conditioning effects could also be produced in NHPs by triggering cortical stimulation
177 from muscle activity [23]. To simulate these experimental results the trigger pulses were
178 obtained from threshold crossings of multiunit EMG activity of Muscle A (Fig 5A). The threshold
179 was chosen such that triggered stimuli were delivered to Column B at a rate comparable to that
180 used for other conditioning methods (approximately 3000 conditioning stimulations over a 500
181 second conditioning period). This paradigm strengthened the synaptic connections from A to B,
182 as shown by the connectivity matrix (Fig 5C) and by the A→B evoked potentials (Fig 5D). The
183 conditioning effect is explained by the computed histogram of spikes in the Ae units aligned
184 with the threshold detection (Fig 5B). This shows a peak in firing of A units that generated the
185 coincident input to the motor units (blue curve) and that preceded the triggered responses in B
186 (red peak).

Fig 5. EMG-triggered stimulation. (A) A conditioning stimulus is applied to all units in Column B at a delay after threshold crossing (θ) in EMG of A motor units. (B) Histograms of Ae and Be unit firing during conditioning aligned with EMG A threshold detection (0 ms). (C) Connection strengths between pre and post synaptic units after conditioning. (D) The average percent increase in the EPs evoked in Column B (orange) and C (blue) from stimulating A as function of delay of EMG-triggered stimulation.

Paired pulse stimulation

Paired pulse conditioning [24,29] was simulated by stimulating Column A followed by stimulation of Column B at a fixed delay (Fig 6A). The resultant connection strengths are shown in Fig 6C for a stimulus delay of 10 ms. Conditioning effects were also documented by delivering test stimuli to Column A and measuring the average EPs in Columns B and C. Fig 6D plots the change in amplitudes of the A→B EPs and A→C EPs as a function of interstimulus delay. Consistent with the bidirectional STDP function, there is a decrease in the size of the EPs for negative conditioning delays (i.e. B stimulated before A), but this is shallower than the peak for positive delays because of the choice for the weakening parameter, which tended to keep synaptic weights small. The histograms of unit firings shows the peak in A spikes produced by the stimulus in A (blue trace) and two peaks in B firing (red trace): the first peak is due to a synaptically relayed response to the A burst and the second is due to the delayed stimulus of B.

Fig 6. Paired pulse stimulation. (A) Pairs of pulses delivered sequentially to A and B with fixed delay. (B) Histogram of Ae and Be unit activity during conditioning aligned with times when first of the paired stimuli occurred (10 ms conditioning delay). (C) Connection strengths

after conditioning. (D) Average percent increase in the evoked potential between the conditioned and unconditioned effect as a function of the interstimulus delay. Insets show the shape of the average EP at conditioning delays of −30 ms and 10 ms. Grey trace plots same for EPs in Column C.

For the same stimulus amplitude, paired pulse conditioning tends to be stronger than spike-triggered conditioning (see Testable outcomes and Fig 10) and does not require correlated bias inputs, since the conditioning pulses themselves evoke strong correlated activity between A and B. The conditioning effect is seen with far fewer conditioning stimuli than used for spike-triggered conditioning, for the same stimulus intensity. Our 500-second conditioning time yielded only 700 paired pulse conditioning stimuli, compared to over 3000 stimuli when using the spike-triggered conditioning method.

In these simulations conditioning effects were obtained by delivering pairs of single pulses. However, in the physiological experiments it was necessary to use a triplet of pulses to obtain effects [24,29]. In the model conditioning with paired triplets of stimuli shows a more potent conditioning effect, which became evident for a range of lower intensities where single stimuli were insufficient (Fig 10).

Cycle-triggered stimulation

To simulate cycle-triggered conditioning [25], episodes of oscillatory beta activity were generated by modulating the bias input to Column B (episodes of 6 oscillations at 20 Hz occurred four times during each 10 second simulation time block). The local field potentials from Column B were filtered with a 15-25 Hz band pass and when this filtered LFP exceeded a

given level, the next zero crossing was either taken as a 0° phase (when rising through zero) or 180° phase (falling through zero) to define the phase of the cycle trigger. During conditioning a stimulus was applied on all units in Column A whenever the cycle trigger for the specified phase occurred in B (Fig 7A). To measure conditioning effects, we applied test pulses on Column A before and after the oscillatory episodes, as in the original experiments. These test pulses could cause a certain amount of tetanic conditioning, but this was lower than the changes caused by the cycle-triggered conditioning.

Fig 7. Cycle-triggered stimulation. (A) A stimulus is applied to Column A at a particular phase of local field potential oscillations in Column B. (B) Post conditioning histogram of Ae and Be units aligned with stimulus trigger at 0 ms. (C) Connection strengths after conditioning with cycle-triggered stimulation at 0° phase. (D) Increase of the evoked responses as a function of stimulation phase. Legend identifies traces for stimulated and recorded columns. Dashed line shows A→B EP increase for tetanic stimulation on Column A with a rate approximately matching that for cycle triggered stimulation.

As shown in Fig 7C, cycle-triggered conditioning at 0° phase shift increased connections from Column A→B and to a lesser extent the connections from Column A→C. In addition, the B→A connections were reduced. Cycle-triggered conditioning at 180° phase shift decreased connections from Column A→B and increased connections from Column B→A (not shown).

Fig 7B shows histograms of unit firings relative to the trigger for stimuli delivered at 0° phase shift. The Ae units fired in response to the stimuli (peak at zero in blue curve). The Be units show the broad oscillatory increase and response to the stimuli (red).

250 Conditioning was also performed with stimuli delivered at other phases. Fig 7D shows how
251 evoked responses vary with conditioning phase for A→B, A→C, and B→A connections.
252 Maximum evoked responses for A→B occurred at about −30°, which matches the phase
253 difference between the bias input modulation and the resulting modulation in the filtered LFP
254 of Column B. Maximum B→A EP responses occurred at about 150° phase shift. The least
255 amount of response occurred with phase shifts between 90° (peak) and 270° (trough) for A→B,
256 and −90° to 90° for B→A.

257 **Control for tetanic stimulation**

258 An important control for conditioning effects is the effect of a comparable amount of open-loop
259 stimulation not triggered by preceding activity. To reduce the effects of such tetanic
260 stimulation, the amount of external bias drive and the area difference between the weakening
261 and strengthening sides of the STDP curve were chosen such that tetanic stimulation, at rates
262 similar to rates for conditioning protocols, did not cause large conditioning effects. The results
263 of tetanic stimulation are shown in Fig 8, for Poisson-distributed stimulation delivered to
264 Column B during the conditioning period. The connection matrices for tetanic stimulation show
265 slight increases over the "no-conditioning" network in the connectivity from Column B to A and
266 B to C (Fig 8A). The changes in connectivity between columns as measured by EP amplitudes
267 are illustrated in Fig 8B and plotted in Fig 8C as a function of stimulus frequency. Tetanic
268 stimulation of B has the greatest effect on connections from B for frequencies between 8 and
269 16 Hz. The EP increases for other connections are small or slightly negative (Fig 8B and C).
270 Most of the conditioning protocols modified the A→B connections with triggered stimulation of
271 Column B. In these cases the conditioned A→B effects were clearly larger than the tetanic

272 effect which had the opposite effect of decreasing A→B EPs. For cycle triggered stimulation
273 where Column A was stimulated, the conditioned effect was larger than the effect of tetanic
274 stimulation of A alone (Fig 7D).

275 **Fig 8. Tetanic stimulation.** (A) Effect on connection strengths of tetanic stimulation of
276 Column B at 5 and 9 Hz (intensity of 2.0 mA), compared to no stimulation. (B) Examples of
277 averaged EPs before and after tetanic stimulation of B at 9 Hz. (C) Mean (over 10 randomized
278 networks) of averaged EP changes produced by tetanic stimulation of B at different
279 frequencies. Legend identifies traces for test-stimulated → EP-recorded columns.

280 **Testable outcomes**

281 Importantly, our IF model can simulate variables and procedures that were not documented in
282 the original physiological experiments. Notably, the strength of synaptic connections in the
283 model was documented by computing stimulus-evoked potentials (Fig 4D-7D and 8C), a test
284 that could in principle be performed experimentally, but is technically difficult. Another
285 comprehensive measure of conditioning effects on synaptic strength is the sum of all the
286 synaptic weights connecting one column to another. There is no feasible physiological or
287 anatomical experiment to measure these weights directly *in vivo*, but they can be readily
288 calculated from the model. Significantly, Fig 9A shows that the computed weight changes
289 closely track the changes in the EPs. Moreover, the weights can be tracked with high temporal
290 resolution, during and after the conditioning to document the induction and decay of the
291 conditioned weight changes. Fig 9B shows the time course of the weight changes in the A→B
292 connections during and after a period of spike-triggered stimulation with STDP. The stimulation

293 is applied during the first 4 seconds of each 10-second time block. The plot of the average time
294 course over 50 blocks shows how the weights tend to increase during the stimulation and then
295 decay towards their preconditioned state after stimulation is turned off.

296 **Fig 9. Network weight measurements.** (A) Comparison between EP increase and mean A→B
297 weight increase for conditioning with spike-triggered stimulation as function of spike-stimulus
298 delay. (B) Average evolution of A→B weights during and after 4 seconds of spike-triggered
299 stimulation at 10 ms conditioning delay.

300 Another testable property that the model can predict is the relative efficacy of conditioning as a
301 function of stimulus intensity and number, as shown for the spike-triggered and paired pulse
302 paradigms in Fig 10. The curve for spike-triggered stimulus pairs rises faster than the curve for
303 spike-triggered single stimuli; this is partly due to the pairs acting as a higher intensity stimulus,
304 but that does not entirely explain the higher asymptote achieved. The curve for paired single-
305 pulse stimulation initially rises more slowly than that for spike-triggered single stimuli, but then
306 surpasses it at 2 mV, our standard conditioning stimulation intensity. The curve for paired
307 triplet stimuli (which had to be used experimentally) rises much faster than that for paired
308 single-pulse stimulation, revealing a stimulus range over which the triplets are more effective
309 than single pulses. The curves asymptote at high stimulus intensities, when most of the units in
310 the stimulated column respond.

311 **Fig 10. Effect of conditioning stimulus amplitudes and trains.** Stimulating with pulse trains
312 (33 ms interstimulus interval) instead of single pulses increases the efficacy of conditioning
313 for spike-triggered stimulation (Spike Trig 2 vs 1) and for paired pulse conditioning (Paired

314 Pulse 3 vs 1) at all stimulus amplitudes. *n* is the total number of stimuli delivered during each
315 simulation. Running the Paired Pulse 1 conditioning longer (n = 3500 compared to n = 700)
316 does not provide the same increase in efficacy as Paired Pulse 3 (n = 714) until efficacy
317 approaches an upper limit at stimulus amplitudes ≥ 2.5 mV.

318 **Testable predictions for novel protocols**

319 Our IF model can also be used to predict outcomes of experiments not yet performed. For
320 example, it is possible to trigger a pulse of *inhibition* of Column B from action potentials of a cell
321 in Column A, which could be achieved by optogenetic spike-triggered inhibition (Fig 11A). The
322 inhibitory effect was modeled as a negative deflection (-2 mV) to the slow decaying part of the
323 membrane potential. The results of this simulation show that the connections from A to B
324 would be reduced (Fig 11D). The trigger-aligned histograms in Fig 11B document the pairing of
325 increases in Ae units with subsequent decreases in B units. The time-course of conditioned
326 reduction in connections as a function of spike-pulse delay roughly resembles the inverse of the
327 increase with spike-triggered stimulation.

328 **Fig 11. Spike-triggered inhibition.** (A) Spikes in one unit in Column A (Ae1) trigger an
329 inhibitory effect on all units in Column B. (B) Perispike histogram of Ae and Be units. (C) Post-
330 conditioning connectivity matrix for 10 ms delay. (D) The standard network parameters yield
331 a relatively mild EP decrease (orange curve). A more active network with 45% correlated bias
332 drive, a weakening value of 0.5, and a −3mV stimulus produces a more robust post-stimulus
333 inhibition (brown).

334 A second untested conditioning paradigm involves triggering stimuli from threshold crossings of
335 *gamma* range LFPs. On the rationale that gamma LFP reflects multiunit activity, these
336 threshold crossings should detect coincident spiking activity that should also produce plasticity.
337 Fig 12 shows the effects of stimuli in B triggered from band-passed mid-gamma LFP in Column A
338 (in 50-80 Hz range). The histogram of Ae unit spikes aligned with the falling gamma threshold
339 crossings (Fig 12B) shows a robust pre-stimulus peak in Ae units (and in LFP A) that generates
340 the threshold crossing. The increase in A→B connections is shown in both the connection
341 matrix (Fig 12C) and in the size of EPs (Fig 12D). Similar effects were found for triggers from
342 high (80-100 Hz) and low range (30-50 Hz) gamma (Fig 12D). Triggering from the rising slope of
343 the gamma activity is associated with a later peak in Ae activity (Fig 12B), consistent with a later
344 latency and a smaller conditioning effect (Fig 12D) than triggering from the falling slope.

345 **Fig 12. Gamma-triggered stimulation.** (A) Stimuli were triggered from threshold crossings of
346 LFP filtered in the gamma frequency ranges shown. (B) Histograms of Ae units (blue) and Be
347 units (red) relative to triggers from falling and rising mid-range gamma filtered LFP in A. Grey
348 curve shows simultaneous LFP in A. (C) Connection strength matrix for falling LFP filtered in
349 mid gamma range (50-80 Hz). (D) changes in EPs for rising and falling threshold crossings for
350 different gamma frequency ranges. Circled points used for histograms in (B).

351 **Relative efficacy of conditioning paradigms**

352 To compare the relative efficacy of different conditioning paradigms, the resulting change of
353 the A→B connections was tested by the change in the EP in B evoked by stimulating A. The
354 results, plotted for different amplitudes of the conditioning stimuli, are shown in Fig 13. The

355 simulations were run with 30% correlated bias drive to the columns. As a control for
356 stimulation alone, the solid gray curve shows the effects of tetanic stimulation of Column B
357 with exponentially distributed stimulation intervals, at the same average rate as the spike-
358 triggered stimulation (blue curve). Above 1.5 mV the other four paradigms all produce stronger
359 effects than spike-triggered stimulation, probably because the stimuli involve larger numbers of
360 Ae spikes. In particular, triggering from EMG and gamma produce larger effects than spike-
361 triggered stimuli above 1 mA because they are selective for coincident Ae spikes (as shown in
362 the histograms in Fig 5B and 12B).

363 **Fig 13. Relative efficacy of conditioning paradigms.** Curves show increase in A→B EP as
364 function of stimulus intensity using standard network parameters. Tetanic stimulation was
365 randomly spaced with rates approximating that for spike-triggered stimulation. Paired pulse
366 interval was 10 ms, same as the spike-trigger delay, while rising EMG and falling gamma
367 trigger delay was 0 ms.

368 Tetanic stimulation of Column B (grey solid curve) is the control for spike-, gamma- and EMG-
369 triggered stimulation of B. Tetanic stimulation of Column A (grey dashed curve) is the control
370 for cycle-triggered stimulation of A (here performed at a phase of 0° in beta cycles). Both
371 tetanic curves are relevant to paired pulse conditioning.

372 The conditioning effects asymptote at stimulus intensities above 2.5 mV, due to maximal
373 activation of units in the stimulated column. The asymptote for spike-triggered stimulation
374 (blue curve) is lower than those of the other conditioning paradigms, but this was a function of

375 the synchrony input driving the Ae units and could be increased by increasing the amount of
376 synchronous relative to asynchronous input drive.

377 **Strengthening disynaptic pathways**

378 The preceding conditioning paradigms focused on changes induced in monosynaptic
379 connections. The degree to which polysynaptic pathways can be modified would be of basic
380 interest and clinical relevance for inducing targeted plasticity to treat lesions. Disynaptic
381 conditioning was investigated for *paired stimulation* of A and B in the absence of direct
382 connections between A and B (Fig 14). The conditioning paradigm is identical to that shown in
383 Fig 6A for paired stimulation of intact networks, but now the most direct pathway between A
384 and B is disynaptic, via Column C (Fig 14A). The weight matrix shows clear increases in A→C
385 and C→B connections after conditioning (Fig 14C). This increase in the disynaptic path was a
386 function of the intensity of the two stimuli, as shown by the increases in A→B EP size plotted
387 for different combinations of intensity in Fig 14B. To produce conditioned changes with pairs of
388 single pulses the stimulation intensity of A had to be at least 3 mV, higher than the typical 2 mV
389 used in other simulations. This was likely necessary so that some tetanic conditioning from
390 A→C would occur (as in Fig 13 Tetanic Col A). However, tetanic stimulation of A alone did not
391 produce a sizeable disynaptic EP (Fig 14B, B stim = 0). The A→B EPs increase appreciably for
392 conditioning with interstimulus delays above 8 ms (Fig 14D), about twice the minimal delay of 4
393 ms for direct connections (Fig 6D).

394 **Fig 14. Disynaptic paired pulse stimulation.** (A) Circuit connections between columns with
395 standard A↔B connections removed. (B) Size of A→B EP as a function of stimulus intensity

396 for the two pulses (for delay of 12 ms). (C) Post-conditioning connection matrix (for A and B
397 stimulus intensities of 3 mA and delay of 12 ms). (D) Size of conditioned A→B EPs as function
398 of paired pulse delays (A and B stimulus intensities of 3 mA).

399 Although larger than standard stimuli were necessary to produce disynaptic conditioning with
400 paired single pulses (Fig 14B), paired triplet stimulation with standard intensities of 2 mV did
401 produce clear disynaptic effects (Fig 16).

402 *Cycle-triggered stimulation* could also be used to strengthen disynaptic connections (Fig 15).
403 The conditioning paradigm is identical to normal cycle-triggered stimulation shown in Fig 7A,
404 but now connections between Column A and Column B have been removed (Fig 15A).
405 Therefore, any EP in Column B caused by a stimulus in Column A must be mediated
406 disynaptically, through Column C. Oscillatory drive was applied only to column B (Fig 15B). The
407 weight matrix again shows that conditioning produced clear increases in A→C and C→B
408 connections (Fig 15C). The stimulation intensity had to be increased to 3.5 mV, more than the
409 typical 2.0 mV used in other simulations. This was probably necessary so that some tetanic
410 conditioning from A→C would occur (as in Fig 13, Tetanic Col A). However, tetanic stimulation
411 of A alone did not produce a sizeable disynaptic A→B EP (Fig 15D, green line).

412 **Fig 15. Disynaptic cycle-triggered stimulation.** (A) Circuit connections between Columns A
413 and B are removed. A stimulus (CT) on Column A is triggered on phases of an oscillatory
414 episode in LFP B. (B) The oscillatory episode in Column B (starting at 0.5 sec) is produced by
415 modulating the probability of external bias spikes to B with a sine wave (7 cycles at 20 Hz). (C)
416 Post conditioning connection matrix shows absence of A↔B connections, and the

417 strengthened A→C and C→B connections that mediate the A→B EP. (D) Conditioned EP sizes
418 for conditioning with different stimulation phases (φ). In contrast to cycle-triggered
419 stimulation with full networks, the B→A EP was slightly depressed and unmodulated with
420 phase. Inset shows A→B EP before (blue) and after (red) conditioning.

421 Disynaptic A→B connections could not be strengthened with spike- or gamma-triggered A→B
422 stimulation, nor with stimulation of B triggered from EMG of Muscle A, even with larger than
423 standard stimulus intensities. These paradigms did strengthen A→C connections, but they did
424 not produce the necessary increase in C→B connections.

425 The above tests involved disynaptic conditioning with A↔B connections deleted. A related
426 question is whether comparable disynaptic conditioning occurs in intact networks as well.
427 Intact networks conditioned with paired triplets using standard 2 mv stimuli (Fig 16A) showed a
428 clear disynaptic bump in the A→B EP (Fig 16B, arrow). Lesioned networks without A↔B
429 connections that were conditioned with paired triplets (Fig 16C) showed a disynaptic A→C→B
430 EP (Fig 16D) whose timing coincided with the delayed bump produced in the intact network.
431 However, their amplitudes differed. To measure the size of the disynaptic EP produced in the
432 intact network we computed the A→C→B EP evoked with the A↔B connections removed for
433 testing. The disynaptic EP produced by conditioning the lesioned networks was about 1.6 times
434 larger than the recovered disynaptic component of the EP in the intact networks, with the
435 identical conditioning protocol.

436 **Fig 16. Paired triplet stimulation with standard 2 mV stimuli.** (A) Intact network. (B) A→B
437 EP after conditioning intact network with 10 ms delay between paired triplets (red) and

before conditioning (blue). Arrow points to disynaptic component of EP. (C) Lesioned network trained without A↔B connections but other connections identical with intact network in (A). (D) A→B EP after conditioning lesioned network. (E) Sizes of intercolumn EPs in 10 conditioned intact and lesioned networks, with different starting weights. X→Y EP refer to monosynaptic A→C and C→B connections (orange and black points) and disynaptic A→C→B EPs (blue points); for the conditioned intact network the disynaptic A→C→B EPs were obtained after removing A↔B connections. Dotted triangles connect corresponding EPs from two starting conditions.

To investigate the reason for this difference we examined the sizes of disynaptic A→C→B EPs and the monosynaptic A→B and C→B EPs for the two networks. To elucidate the effects of initial weight choices on these values, this comparison was done for 10 intact networks (each starting with different initial synaptic weights) and 10 lesioned networks that had identical initial weights except with A↔B connections deleted before conditioning (with paired triplets). Fig 16E plots the relative sizes of these EPs produced in the 10 networks. The disynaptic A→C→B EPs in the intact and lesioned networks (blue points) are proportional, with a linear slope of 1.57. The monosynaptic A→C and C→B connections (orange and black points) were also proportional, with slopes of 0.81 and 1.61, respectively. The two dotted triangles connect three corresponding EPs for two initial conditions (the ones that produced the largest and smallest EPs). The plots illustrate the variation in absolute sizes that can emerge from different starting points and also show that the sizes of the 3 EPs covary. These plots show that the larger disynaptic EP in the lesioned network can be attributed to a larger increase in the C→B connections.

460

461 **Discussion**

462 Our IF model captures the experimental outcomes from four different conditioning paradigms
463 experimentally investigated in motor cortex of awake NHPs. A powerful feature of the model is
464 to explore estimates of many variables that were not measured in the original experiments,
465 such as changes in the connection matrices, sizes of evoked potentials (which measure the
466 synaptic strength of inter-column connections), and peristimulus histograms of neural activity.
467 Furthermore, the model predicts the outcomes of novel experiments not yet performed.

468 In comparison, a previous neural network model used populations of Poisson firing units and
469 STDP to analytically compute the population effects produced by spike-triggered stimulation
470 [26]. That model replicated the experimental results on net changes in connectivity and
471 showed that the amount of conditioning was dependent on the correlations between units.
472 Their model predicted that conditioning efficacy would be greater when cross-correlation peaks
473 were wider, as they typically are during sleep compared to waking. In contrast, our IF model is
474 based on simulating the synaptic connections between excitatory and inhibitory spiking
475 neurons that integrate synaptic inputs to firing threshold. Our IF network provides cellular
476 resolution of conditioning effects and their dependence on network parameters and simulates
477 many different conditioning protocols.

478 A similar approach was used to model conditioning with spike-triggered stimulation in
479 somatosensory cortex of NHPs [21]. That study examined the effect of spike-triggered and
480 random microstimulation on firing rates and mutual information in S1. A large network of

481 biophysical units with STDP reproduced many of the global physiological findings. In contrast,
482 our smaller network of much simpler IF units was sufficient to replicate relatively detailed
483 spatiotemporal measures of conditioning effects.

484 Other modelling studies have combined IF networks with STDP to investigate related issues.
485 Adding a STDP rule to large populations of conductance-based units [12] led to the emergence
486 of interconnected groups under steady-state conditions [17]. Our model had fewer units with
487 predetermined connections between groups, and reached an equilibrium steady state under
488 STDP before conditioning procedures were introduced. Another large-scale cortical network
489 model showed that realistic synaptic plasticity rules coupled with homeostatic mechanisms led
490 to the formation of neuronal assemblies that reflect previously experienced stimuli [19].

491 Bono and Clopath investigated STDP and dendritic spike mechanisms in producing plasticity in
492 biophysically realistic neural models [18]. Another study showed that STDP rules had to be
493 augmented with mechanism for heterosynaptic competition to generate networks capable of
494 producing sequences of neural activity [30]. On the behavioral level, a model of orbitofrontal
495 networks of IF units with STDP learned the rules of goal-directed actions [20]. These studies
496 investigated various functional issues, in contrast to our focus on mechanisms of synaptic
497 plasticity.

498 **Differences between the IF model and physiological mechanisms**

499 It seems remarkable that our simple voltage-based IF model could replicate the results of many
500 different physiological conditioning experiments. This robust performance raises the question
501 of where the model has limitations that would require further refinement. There are several

502 differences between the performance of our model and the original physiological conditioning
503 experiments. First, in the cortical spike-triggered stimulation experiments, not all site pairs
504 developed strengthened connections [22,27]. This may simply be due to a lack of sufficient
505 synaptic connections between those sites to strengthen. However, this explanation would not
506 apply to the original paired stimulation experiments [24], in which many pairs of sites did seem
507 to have sufficient synaptic connections to mediate EPs, but these did not show conditioned
508 changes. Second, with paired stimulation *in vivo* a minimum of three pulses was required to
509 produce conditioned changes [24,29]. In contrast, our IF model exhibited reliable conditioning
510 even with pairs of single pulses, although triplet stimulation was substantially more potent than
511 pairs of single stimuli over a range of intensities. The need for triplet instead of single pulses *in*
512 *vivo* and the lack of conditioning effects for certain cortical sites remain to be better
513 understood before these physiological observations can inform a change in the model.

514 It seems possible that more sophisticated models, such as a network of biophysically more
515 realistic units would help address some of these limitations. For example, the conductance-
516 based units of Izhikevich capture biophysical properties that can replicate the complex firing
517 properties of many types of cortical neurons in response to prolonged current injection [12,21].
518 It will be interesting to use the conductance-based units with STDP to simulate the different
519 conditioning paradigms investigated here. This will require decisions about the number and
520 connectivity of specific types of units in such a model as well as their biophysical parameters.
521 The fact that our simple voltage-based IF network replicates the overall experimental
522 observations may be related to two factors. It may represent an effective and sufficient
523 average of the different types of biophysical neurons involved in the *in vivo* experiments.

524 Second, the different response properties of biophysical units that can be demonstrated with
525 prolonged intracellular or synaptic drive may be less critical for the phasic events that underly
526 these conditioning protocols.

527 Our model used a STDP rule that required pre- and post-synaptic spikes to generate a change in
528 synaptic connections. Physiological synapses could also be strengthened when the
529 postsynaptic cell is merely depolarized after arrival of the presynaptic spike [15]. This would
530 represent a plasticity paradigm that does not require post-synaptic spikes. This mechanism
531 would contribute to conditioning with cycle-triggered stimulation, for example. Intracellular
532 recordings *in vivo* indicate that many cortical neurons show periodic membrane depolarization
533 during beta oscillations that do not reach threshold for spiking [31,32]. Phase-locked
534 stimulation would modify the strength of synaptic connections to these depolarized neurons as
535 well as to spiking neurons. This may explain the slight difference in the phase for maximum
536 conditioning effects. Our simulations did not track the depolarization level of each unit, so the
537 results of this STDP mechanism remain to be investigated in a future study.

538 **Parameter choices**

539 The performance of our IF model depends of course on the choice of parameters. One choice
540 involves the strength of baseline *synaptic connections*. To capture the small unitary synaptic
541 potentials between cortical neurons [33,34] the plasticity parameters chosen for our model
542 tend to produce a steady-state network with small connections when no activity-dependent
543 conditioning protocol is in effect. This limits the effects produced by tetanic stimulation alone
544 and makes conditioned increases in weights relatively robust. However, it also limits

545 conditioned decreases in weights, since the starting size for most weights is already small. A
546 possible future direction would be to develop a method to encourage a steady state of
547 moderate weights so that both strengthening and weakening effects can manifest more
548 equitably. This might also allow for more effects to emerge from inhibitory units, which play
549 very little role in the network simulations shown here. We found that IF networks that were
550 run without inhibitory units showed conditioning responses similar to networks that had many
551 inhibitory connections.

552 A second choice in our model was using the same *STDP function* for inhibitory and excitatory
553 units. The STDP function for inhibitory neurons has been found to vary, depending on the
554 specific types of source and target neurons [13,15,35,36]. We decided to use the same STDP
555 function for both, which has empirical support [37], and to leave the consequences for different
556 functions for inhibitory units, such as symmetric functions, to be explored in another study.
557 Moreover, our STDP rule is based on pairs of pre- and post-synaptic spikes; models with "multi-
558 spike" STDP interactions can produce different network dynamics [38].

559 A third choice in our model involved the relative amount of *external correlated input* bias. High
560 amounts of correlated input can cause sufficient synchrony to strengthen connections from
561 that column even in the absence of conditioning. As the percent of correlated biases increases,
562 the weakening portion of the STDP curve may be increased to prevent this effect from
563 interfering with the manifestation of conditioning effects. For example, in our networks, the
564 weakening value of 0.55 showed a spontaneous conditioning effect with 50% correlated/50%
565 uncorrelated bias inputs, but did not show this effect with our chosen 30% correlated biases.

566 In general, our choice of network parameters was guided by achieving realistic physiological
567 performance. Notably, the same set of parameters was used to simulate all four conditioning
568 paradigms. Network performance was generally stable for modest deviations from the chosen
569 parameters. The consequences of larger variations in different parameters would be
570 interesting to explore but are beyond the scope of this report.

571 **Modeled connectivity and activity**

572 An informative use of the model is to simulate activity and network connectivity that were not
573 measured in the original experiments but that elucidate associated mechanisms. For example,
574 calculating the EPs provides an easy and experimentally feasible measure of net connectivity
575 between sites and can reveal its dependence on conditioning parameters like stimulus
576 amplitude and delay, synchrony, etc. The changes to connection weights themselves can be
577 computed in the model (but not experimentally); these weights closely tracked the EP measure
578 (Fig 9A). The weights further revealed a better time-resolved prediction of the induction and
579 decay of these synaptic connections (Fig 9B).

580 A particularly useful insight from the model is the activity of relevant units around the stimulus
581 trigger events. Their stimulus-aligned histograms reveal why EMG-triggered and gamma-
582 triggered stimulation are such effective conditioning paradigms: they both select for coincident
583 unit activity, as shown by the preceding peak in activity of A units (Fig 5B and 12B). This peak
584 preceding the stimulus-evoked post-synaptic activity in B is responsible for the strengthening of
585 the A→B connections.

586 **Testable predictions**

587 A possible therapeutic application of closed-loop conditioning is to strengthen polysynaptic
588 pathways as well as strengthen direct connections. Such targeted plasticity could restore
589 functional pathways lost to injury or stroke [39]. The model was used to examine conditioning
590 of *disynaptic* links by performing A-B paired-pulse conditioning in a network without direct A-B
591 connections and looking for development of A→C→B connections. This did occur, as shown by
592 development of relevant disynaptic evoked potentials after conditioning and by the
593 connectivity matrix (Fig 14). Similarly, cycle-triggered stimulation could also strengthen
594 disynaptic connections (Fig 15); however, this paradigm would be significantly more challenging
595 to apply *in vivo* than paired stimulation. Both paradigms involved sufficient stimulation of A to
596 strengthen A→C connections. The other 3 paradigms involved only stimulation of B and did not
597 strengthen disynaptic A→C→B links. Another significant prediction of the model is that
598 disynaptic effects are conditioned more robustly between sites that lack direct connections as
599 compared to sites that also have direct connections. These simulations provide useful
600 predictions of effective targeted plasticity paradigms and parameters to strengthen
601 polysynaptic pathways.

602 The model also predicts several conditioning paradigms that improve on methods used to date.
603 Instead of spike-triggered single stimuli, the use of spike-triggered *bursts of stimuli* is more
604 effective, increasing with the number of stimuli (Fig 10). Second, *gamma-triggered stimulation*
605 is more effective than spike-triggered stimulation because it detects coincident spikes that
606 produce the gamma threshold crossing. Importantly, gamma-triggered stimulation is
607 experimentally much easier to perform *in vivo* because it does not require long-term isolation

608 of single action potentials. An important caveat here is that the model assumes that gamma is
609 generated in a large number of A units that are synchronized and also connected to the B units.
610 The efficacy of gamma-triggered conditioning would decrease if fewer units generating the
611 gamma LFP in A sent connections to the stimulated units. Preliminary tests of this paradigm by
612 R. Yun (unpublished) indicate that conditioning effects are less robust *in vivo* in NHP motor
613 cortex than in the model. This indicates that the connectivity of our network, designed to
614 separate the recorded, stimulated and control groups may be too simple to accurately predict
615 experimental outcomes for more complex biological networks in which these functional groups
616 are intermingled with many other connectivities.

617 **Concluding comments**

618 The simple IF spiking network described here has proven remarkably effective in capturing
619 experimental results previously obtained in NHPs with four different conditioning paradigms,
620 including three with closed-loop activity-dependent stimulation. In addition to replicating the
621 observed phenomena, the model also allows computation of underlying network behavior and
622 correlated changes not originally documented. The model also makes significant predictions
623 about protocols not yet investigated, including triggering bursts instead of single stimuli and
624 gamma-triggered stimulation. The success of these simulations suggests that a simple voltage-
625 based IF model incorporating STDP is sufficient to capture the essential mechanisms that
626 produce targeted plasticity. Further detailed comparisons with physiological experiments will
627 likely inform development of models with more realistic connectivity and biophysical
628 properties.

Methods

Integrate-and-fire network model

The cortical network model is comprised of 240 integrate-and-fire units. Each unit maintains a potential $V_i(t)$ which represents the sum of the synaptic inputs from units with connections to unit *i* (Fig 1A). $V_i(t)$ is calculated at discrete time steps of 0.1 ms. When $V_i(t)$ exceeds a threshold θ, the unit "fires" and its spike function $U_i(t)$ is set to 1 for that time step (Eq 3). Each time a unit fires, its potential is reset to zero on the next time step and an output spike is initiated from that source unit to all its target units.

The responses of the modeled units to spiking inputs represent the post-synaptic potentials (PSPs) of physiological neurons (Fig 1B). The form of the PSP is calculated as the difference between two exponential decay functions as follows.

$$PSP(t) = w\left(e^{-(t-t_{spike})/\tau_s} - e^{-(t-t_{spike})/\tau_f}\right), \text{ if } t \geq t_{spike}\text{ ;0 otherwise} \quad \textbf{(1)}$$

The time constants τ_s (slower decay) and τ_f were chosen to give reasonably shaped PSPs, rising rapidly from zero to a maximum, and then decaying more slowly back towards zero (Fig 1B). The parameter *w* is the connection *weight* -- this parameter is modified by the plasticity calculations. A related parameter, the connection *strength* is measured by the PSP maximum, which represents the synaptic efficacy in voltage change, relatable to distance to threshold. The relation between the weight and strength depends on τ_s and τ_f (Fig 1B). The calculation of $V_i(t)$ is greatly simplified by using the same value of τ_s and τ_f for all connections. This allows $V_i(t)$

to be represented by two leaky integrators $V^s_i(t)$ and $V^f_i(t)$ that decay with these constants (Eq 4, 5); they both receive the same spiking input and reset with the same spike time function $U_i(t)$. Here the Euler method is used to estimate the exponential decay functions. We let $A_i(t)$ be the sum of all incoming spike activity to unit *i* at time *t* (Eq 6), and then calculate the unit potential $V_i(t)$ and spike time function $U_i(t)$ as follows.

$$V_i(t) = V_i^s(t) - V_i^f(t) \tag{2}$$

$$U_i(t) = 1, \text{ if } V_i(t) > \theta; 0 \text{ otherwise} \tag{3}$$

$$V_i^s(t+h) = (1 - h/\tau_s)\, V_i^s(t) + A_i(t), \text{ if } U_i(t) = 0; 0 \text{ if } U_i(t) = 1 \tag{4}$$

$$V_i^f(t+h) = (1 - h/\tau_f)\, V_i^f(t) + A_i(t), \text{ if } U_i(t) = 0; 0 \text{ if } U_i(t) = 1 \tag{5}$$

Each connection linking source unit *j* to target unit *i* at time *t* is defined by a weight $w_{ij}(t)$. Non-existent connections assume a weight of 0. Axonal plus dendritic conduction times are modeled as a global delay parameter *d* for all connections. To provide additional background activity each unit also receives external input $E_i(t)$ the sum of all external spiking activity arriving at unit *i* at time *t* (Eq 7). $A_i(t)$ is defined as follows:

$$A_i(t) = E_i(t) + \sum_{j=1}^{n} \left(U_j(t-d) \cdot w_{ij}(t)\right) \tag{6}$$

where *n* equals the total number of units. The units are subdivided into three populations called "columns", representing recorded, stimulated and control sites (see below). To provide

background spontaneous activity, each column receives excitatory external inputs $E_i(t)$ that are a combination of correlated inputs $E^c_i(t)$ and uncorrelated inputs $E^u_i(t)$.

$$E_i(t) = E_i^c(t) + E_i^u(t) \tag{7}$$

These inputs produce PSPs with the same waveform as other connections in the network, varying only in amplitude. For each column, the correlated events occur with a given probability at each time step; every unit in the column receives the correlated input at a random time within a Gaussian distribution with a standard deviation of 3 ms. Uncorrelated events occur with a separate independent probability at every time step for each unit. The delivery probabilities of correlated and uncorrelated events can be modulated in time to simulate different dynamics of background activity (e.g. oscillations). For our networks $E^c_i(t)$ and $E^u_i(t)$ assume a fixed connection weight at times of external spike delivery and are 0 otherwise.

Plasticity rule

When spike-timing dependent plasticity is active, connection weights are modified based on the relative firing times of the target and source units. The STDP Curve (Fig 1C) shows how much weight w_{ij} changes as a function of the difference in spike times between target unit *i* and source unit *j*. The curve has two components: a strengthening portion for positive differences Δt between time of postsynaptic spike and arrival of presynaptic spike that will strengthen the weight, and a weakening portion for negative time differences that will weaken the weight. Each half of the STDP function was approximated with exponential decay functions similar to

693 the PSP function except with longer time constants (a_s, a_f, b_s, b_f) and with amplitudes controlled

694 by the training factor r and a weakening factor c.

695 $$STDP(\Delta t) = \begin{cases} r\left(e^{-\Delta t/a_s} - e^{-\Delta t/a_f}\right), & \Delta t \geq 0 \\ -cr\left(e^{\Delta t/b_s} - e^{\Delta t/b_f}\right), & \Delta t < 0 \end{cases}$$

696 **(8)**

697 The weakening side of the STDP curve has a lower amplitude but decays more slowly than the

698 strengthening side, and has larger overall area [13]. The same STDP function was used for

699 excitatory and inhibitory synaptic connections, for which there is empirical support [37]. For

700 further discussion of this and alternate STDP functions for inhibitory synapses, see Discussion.

701 Choosing the right amount of weakening vs strengthening is important to the evolution of the

702 network connections. If the weakening factor is too small, the greater area of the

703 strengthening side of the STDP curve will eventually cause all weights to grow to a maximum

704 limit. If the weakening factor is too high, the greater area of the weakening side will push all

705 weights strongly toward zero. We chose a weakening factor of c = 0.55, so that the network

706 sustained low weight values in the absence of any conditioning stimuli but showed noticeable

707 increases in some weights when conditioning was applied.

708 For a single weight w_{ij} and time difference between spikes of unit i and arriving spikes of unit j,

709 the change in w_{ij} is equal to the value taken from the STDP function in Fig 1C. To facilitate

710 computation of weight changes, strengthening and weakening potentials are maintained for

711 each unit similar to the way unit potential $V_i(t)$ sums PSPs (except with no threshold crossing

712 reset). $S_j(t)$ sums the strengthening side of the STDP curve for each source unit j using time

713 constants a_s and a_f with input activity $U_j(t - d)$. $T_i(t)$ sums the weakening side for each target

unit *i* using time constants b_s and b_f with input activity $U_i(t)$. Thus, when a spike occurs, weight changes can be calculated with respect to previous spikes by taking signed and scaled values of $S_j(t)$ and $T_i(t)$ (Eq 15).

$$S_j(t) = S_j^s(t) - S_j^f(t) \tag{9}$$

$$S_j^s(t+h) = (1 - h/a_s)\, S_j^s(t) + U_j(t-d) \tag{10}$$

$$S_j^f(t+h) = (1 - h/a_f)\, S_j^f(t) + U_j(t-d) \tag{11}$$

$$T_i(t) = T_i^s(t) - T_i^f(t) \tag{12}$$

$$T_i^s(t+h) = (1 - h/b_s) T_i^s(t) + U_i(t) \tag{13}$$

$$T_i^f(t+h) = (1 - h/b_f)\, T_i^f(t) + U_i(t) \tag{14}$$

The change to w_{ij} at a given time step is:

$$\Delta w_{ij}(t) = r\, \mathrm{sgn}\big(w_{ij}(t)\big)\big(S_j(t)\, U_i(t) - c\, T_i(t)\, U_j(t-d)\big) \tag{15}$$

$$w_{ij}\,(t+h) = F\big(w_{ij}(t) + \Delta w_{ij}(t)\big) \tag{16}$$

735 The function *F(w)* clips excitatory weights to the range $w_{min} \leq w \leq w_{max}$, and inhibitory weights

736 to the range $-w_{max} \leq w \leq -w_{min}$. The standard parameter values used in simulations are shown in

737 Table 1.

738

739 **Table 1. Standard parameter values.**

Number of excitatory units in each column	40
Number of inhibitory units in each column	40
Unit firing threshold	5 mV
Conduction delay between cortical units	3 ms
Conduction delay to motor outputs	10 ms
External input PSP size	350 µV
Unit potential time constants τ_s, τ_f	3.2 ms, 0.8 ms
External input rate	1800 spikes per second
External input correlated/uncorrelated rate	0.3
External input correlated event standard deviation	3 ms
Training factor *r*	100
Weakening factor *c*	0.55
STDP strengthening curve time constants a_s, a_f	15.4 ms, 2 ms
STDP weakening curve time constants b_s, b_f	33.3 ms, 2 ms
Conditioning stimulus size	2 mV
Maximum connection strength	500 µV
Minimum weight w_{min}	1
Probability of excitatory cortical connections	1/6
Probability of inhibitory connections	1/3
Probability of corticomotoneuronal connections	1/3
Number of motoneurons in each column	40
Motoneuron thresholds	5 to 6 mV
Motor unit potential size	0.5 to 1.5 mV

740

741 **Network topology**

742 Cortical units were grouped into three columns: A, B, and C, as shown in Fig 2A. Each column

743 has 40 excitatory units (e) that project only positive weights, and 40 inhibitory units (i) that

project only negative weights. Excitatory units connect sparsely to all other units in the network and inhibitory units connect less sparsely to all cortical units within the same column. The probability of each possible connection is listed in Table 1. Unit self-connections are not allowed. Each column also has a simulated local field potential (LFP) which is the sum of all post-synaptic potentials occurring within a column.

To provide background spontaneous activity each column receives an external excitatory bias input generated separately for each column. Some bias inputs provide correlated spikes to each unit in a column, and others provide independent uncorrelated spikes to all units (C and U in Fig 2A), for a combined mean bias rate of 1800 spikes/sec to each unit. The ratio of the number of correlated to uncorrelated spikes each unit receives can be modified to control the degree of synchronization within a column. The mean bias rate can also be modulated over time, for example to generate oscillatory activity or simulate behavioral activation.

To simulate experiments that involved recording muscle activity, the network includes pools of motor units driven by the cortical columns (Fig 2B). Associated with each column is a pool of 40 motoneurons that receive inputs from a third of the excitatory units of that column, as well as from uncorrelated external drive to simulate all additional inputs. Consistent with the size principle [40], the pool included a range of small to large motoneurons, with increasing thresholds from 5 to 6 mV and increasing muscle unit potentials from 0.5 to 1.5 mV. Multiunit electromyographic (EMG) activity was simulated by summing all the muscle unit potentials in the same manner as for unit PSPs and then filtering the result with a 100 to 2500 Hz bandpass filter.

765 Fig 2C shows the simulated spiking activity of all units under steady-state conditions. Also
766 plotted are the corresponding LFPs for each column. The coordinated bursts of activity are
767 produced by 30% correlated external bias drive.

768 **Conditioning stimulation**

769 The effect of electrical stimulation on a stimulated unit is modeled by a large and immediate
770 deflection of its potential towards threshold, computed by adding a large stimulus pulse to the
771 unit's $V^s_i(t)$, proportional to stimulus intensity. The standard conditioning stimulus produces a
772 step in V_i(t) of amplitude 2ma. The standard testing stimulus for evoking EPs produces a step in
773 V_i(t) of amplitude 3ma. Normally a conditioning stimulus is applied to all units in a column
774 simultaneously, causing many of them to fire. This burst of spikes will evoke a measurable
775 response in the LFP of other columns, called the Evoked Potential (EP). The EP is a measure of
776 the net synaptic strengths from the stimulated column to the recorded column. The size of
777 each EP is calculated as the difference between the amplitude of the LFP peak after the
778 stimulus compared to pre-stimulation baseline LFP. The average change in the EP amplitude
779 produced by conditioning is quantified as the percent increase of the average EP amplitude
780 after conditioning compared to before conditioning (Eq 17).

781 $$EP\ Increase\ \% = \frac{100\ (Post\ Conditioned\ Average\ EP - Preconditioned\ Average\ EP)}{Preconditioned\ Average\ EP}$$
782 **(17)**

783 **Implementation**

784 The network has many modifiable parameters that can affect the outcome of a simulation
785 (Table 1). Temporal parameters are generally scaled in milliseconds. The network runs in time

786 steps of 0.1 ms to strike a balance between accuracy and computation time. Connection
787 strengths, stimulation amplitudes, and PSP-related parameters are scaled in microvolts to
788 relate such values to physiological variables. Connection strengths are initially small values (20
789 to 60 percent of maximum) taken randomly from a uniform distribution.

790 Most networks were run in 10-second time blocks for 2000 seconds of simulated time, divided
791 into four periods of 500 seconds each (Table 2). During the preconditioning period STDP is on
792 and the network settles into an unconditioned steady state. During the two testing stages
793 before and after conditioning the STDP calculations are turned off, allowing graphs and tests to
794 be compiled while the network runs with static weights. The conditioning paradigm is run
795 during the conditioning period with STDP on.

796 **Table 2. Sequential training periods.**

Period	Preconditioning	Precondition Testing	Conditioning	Post Condition Testing
Plasticity	On	Off	On	Off
Conditioning	Off	Off	On	Off

797

798 **Tetanic stimulation**

799 To control for the effects of stimulation alone, tetanic stimulation was performed with a 10 Hz
800 Poisson spike train with an imposed 10 ms refractory period. This can have a strengthening
801 effect on connections from the stimulated column to the other two columns, and a weakening
802 effect in the reciprocal directions. These effects were minimized by selecting a weakening
803 factor large enough to yield preconditioned networks with small weights that would readily
804 show the effects of strengthening conditioning methods (Fig 8A). There is substantial variation

in the sizes of conditioned EPs (Fig 8B) due to differences in initial conditions, the randomness of the external input, and the magnitude of the training factor parameter. However, averaging over a set of simulations using 10 different initial conditions yield a reliable measure of the effects of tetanic stimulation (Fig 8C). These tetanic effects can support or oppose other conditioning methods. For example, any paradigm to strengthen A→B connections that employs stimulation on Column B must overcome the tendency for tetanic stimulation on B to weaken those connections. On the other hand, paradigms that stimulate Column A (like cycle-triggered stimulation) should be evaluated relative to simple tetanic stimulation of Column A.

Source code

The Matlab source code for the IF network model is available on the website https://depts.washington.edu/fetzweb/ifnetwork.html. This includes documentation and instructions on running the model as well as further explanation of effects of network parameters.

Acknowledgements

We thank Drs. Adrienne Fairhall and Guillaume Lajoie for helpful comments on the manuscript.

822 ## References

823 1. Fetz EE. Dynamic recurrent neural network models of sensorimotor behavior. In: Gardner
824 D, editor. THE NEUROBIOLOGY OF NEURAL NETWORKS. Cambridge MA: MIT Press; 1993.
825 p. 165 - 90.
826 2. Fetz EE, Shupe LE. Dynamic models of neurophysiological systems. In: Arbib M, editor.
827 HANDBOOK OF BRAIN THEORY AND NEURAL NETWORKS. Cambridge, MA: MIT Press;
828 1995. p. 332 - 5.
829 3. Gerstner W, Kistler WM. Spiking Neuron Models. Single Neurons, Populations, Plasticity:
830 Cambridge University Press; 2002.
831 4. Neuronal Dynamics; https://neuronaldynamics.epfl.ch (Internet). 2014. Available from:
832 https://neuronaldynamics.epfl.ch/online/.
833 5. Burkitt AN. A review of the integrate-and-fire neuron model: I. Homogeneous synaptic
834 input. Biol Cybern. 2006;95(1):1-19.
835 6. Gilson M, Burkitt AN, Grayden DB, Thomas DA, van Hemmen JL. Emergence of network
836 structure due to spike-timing-dependent plasticity in recurrent neuronal networks IV:
837 structuring synaptic pathways among recurrent connections. Biol Cybern. 2009;101(5-
838 6):427-44.
839 7. Gilson M, Burkitt AN, Grayden DB, Thomas DA, van Hemmen JL. Emergence of network
840 structure due to spike-timing-dependent plasticity in recurrent neuronal networks. I.
841 Input selectivity--strengthening correlated input pathways. Biol Cybern. 2009;101(2):81-
842 102.

843 8. Gilson M, Burkitt AN, Grayden DB, Thomas DA, van Hemmen JL. Emergence of network
844 structure due to spike-timing-dependent plasticity in recurrent neuronal networks. II.
845 Input selectivity--symmetry breaking. Biol Cybern. 2009;101(2):103-14.
846 9. Gilson M, Burkitt AN, Grayden DB, Thomas DA, van Hemmen JL. Emergence of network
847 structure due to spike-timing-dependent plasticity in recurrent neuronal networks III:
848 Partially connected neurons driven by spontaneous activity. Biol Cybern. 2009;101(5-
849 6):411-26.
850 10. Jolivet R, Lewis TJ, Gerstner W. Generalized integrate-and-fire models of neuronal
851 activity approximate spike trains of a detailed model to a high degree of accuracy. J
852 Neurophysiol. 2004;92(2):959-76.
853 11. Ponulak F, Kasinski A. Introduction to spiking neural networks: Information processing,
854 learning and applications. Acta Neurobiol Exp (Wars). 2011;71(4):409-33.
855 12. Izhikevich EM. Simple model of spiking neurons. IEEE Trans Neural Netw.
856 2003;14(6):1569-72.
857 13. Caporale N, Dan Y. Spike timing-dependent plasticity: a Hebbian learning rule. Annu Rev
858 Neurosci. 2008;31:25-46.
859 14. Feldman DE. The spike-timing dependence of plasticity. Neuron. 2012;75(4):556-71.
860 15. Markram H, Gerstner W, Sjostrom PJ. Spike-timing dependent plasticity: a
861 comprehensive overview. Frontiers in Computational Neuroscience. 2012:1-574.
862 16. Bi G, Poo M. Synaptic modification by correlated activity: Hebb's postulate revisited.
863 Annu Rev Neurosci. 2001;24:139-66.

17. Izhikevich EM, Gally JA, Edelman GM. Spike-timing dynamics of neuronal groups. Cereb Cortex. 2004;14(8):933-44.
18. Bono J, Clopath C. Modeling somatic and dendritic spike mediated plasticity at the single neuron and network level. Nat Commun. 2017;8(1):706.
19. Litwin-Kumar A, Doiron B. Formation and maintenance of neuronal assemblies through synaptic plasticity. Nat Commun. 2014;5:5319.
20. Koene RA, Hasselmo ME. An integrate-and-fire model of prefrontal cortex neuronal activity during performance of goal-directed decision making. Cereb Cortex. 2005;15(12):1964-81.
21. Song W, Kerr CC, Lytton WW, Francis JT. Cortical plasticity induced by spike-triggered microstimulation in primate somatosensory cortex. PLoS One. 2013;8(3):e57453.
22. Jackson A, Mavoori J, Fetz EE. Long-term motor cortex plasticity induced by an electronic neural implant. Nature. 2006;444(7115):56-60.
23. Lucas TH, Fetz EE. Myo-cortical crossed feedback reorganizes primate motor cortex output. J Neurosci. 2013;33(12):5261-74.
24. Seeman SC, Mogen BJ, Fetz EE, Perlmutter SI. Paired Stimulation for Spike-Timing-Dependent Plasticity in Primate Sensorimotor Cortex. J Neurosci. 2017;37(7):1935-49.
25. Zanos S, Rembado I, Chen D, Fetz EE. Phase-Locked Stimulation during Cortical Beta Oscillations Produces Bidirectional Synaptic Plasticity in Awake Monkeys. Curr Biol. 2018;28(16):2515-26 e4.

884 26. Lajoie G, Krouchev NI, Kalaska JF, Fairhall AL, Fetz EE. Correlation-based model of
885 artificially induced plasticity in motor cortex by a bidirectional brain-computer interface.
886 PLoS Comput Biol. 2017;13(2):e1005343.
887 27. Rebesco JM, Stevenson IH, Kording KP, Solla SA, Miller LE. Rewiring neural interactions by
888 micro-stimulation. Front Syst Neurosci. 2010;4.
889 28. Nishimura Y, Perlmutter SI, Eaton RW, Fetz EE. Spike-timing-dependent plasticity in
890 primate corticospinal connections induced during free behavior. Neuron.
891 2013;80(5):1301-9.
892 29. Rebesco JM, Miller LE. Altering function in cortical networks by short-latency, paired
893 stimulation. Conf Proc IEEE Eng Med Biol Soc. 2010;2010:1674-7.
894 30. Fiete IR, Senn W, Wang CZ, Hahnloser RH. Spike-time-dependent plasticity and
895 heterosynaptic competition organize networks to produce long scale-free sequences of
896 neural activity. Neuron. 2010;65(4):563-76.
897 31. Chen D.F. Synaptic interactions between primate cortical neurons revealed by in vivo
898 intracellular potentials. Seattle, WA: University of Washington; 1993.
899 32. Fetz EE, Chen D, Murthy VN, Matsumura M. Synaptic interactions mediating synchrony
900 and oscillations in primate sensorimotor cortex. J Physiol Paris. 2000;94(5-6):323-31.
901 33. Matsumura M, Chen D, Sawaguchi T, Kubota K, Fetz EE. Synaptic interactions between
902 primate precentral cortex neurons revealed by spike-triggered averaging of intracellular
903 membrane potentials in vivo. J Neurosci. 1996;16(23):7757-67.
904 34. Markram H, Lubke J, Frotscher M, Sakmann B. Regulation of synaptic efficacy by
905 coincidence of postsynaptic APs and EPSPs. Science. 1997;275(5297):213-5.

906 35. Kullmann DM, Lamsa KP. LTP and LTD in cortical GABAergic interneurons: emerging rules
907 and roles. Neuropharmacology. 2011;60(5):712-9.
908 36. Vogels TP, Sprekeler H, Zenke F, Clopath C, Gerstner W. Inhibitory plasticity balances
909 excitation and inhibition in sensory pathways and memory networks. Science.
910 2011;334(6062):1569-73.
911 37. Haas JS, Nowotny T, Abarbanel HD. Spike-timing-dependent plasticity of inhibitory
912 synapses in the entorhinal cortex. J Neurophysiol. 2006;96(6):3305-13.
913 38. Babadi B, Abbott LF. Stability and Competition in Multi-spike Models of Spike-Timing
914 Dependent Plasticity. PLoS Comput Biol. 2016;12(3):e1004750.
915 39. Guggenmos DJ, Azin M, Barbay S, Mahnken JD, Dunham C, Mohseni P, et al. Restoration
916 of function after brain damage using a neural prosthesis. Proc Natl Acad Sci U S A.
917 2013;110(52):21177-82.
918 40. Henneman E, Somjen G, Carpenter DO. Functional Significance of Cell Size in Spinal
919 Motoneurons. J Neurophysiol. 1965;28:560-80.
920

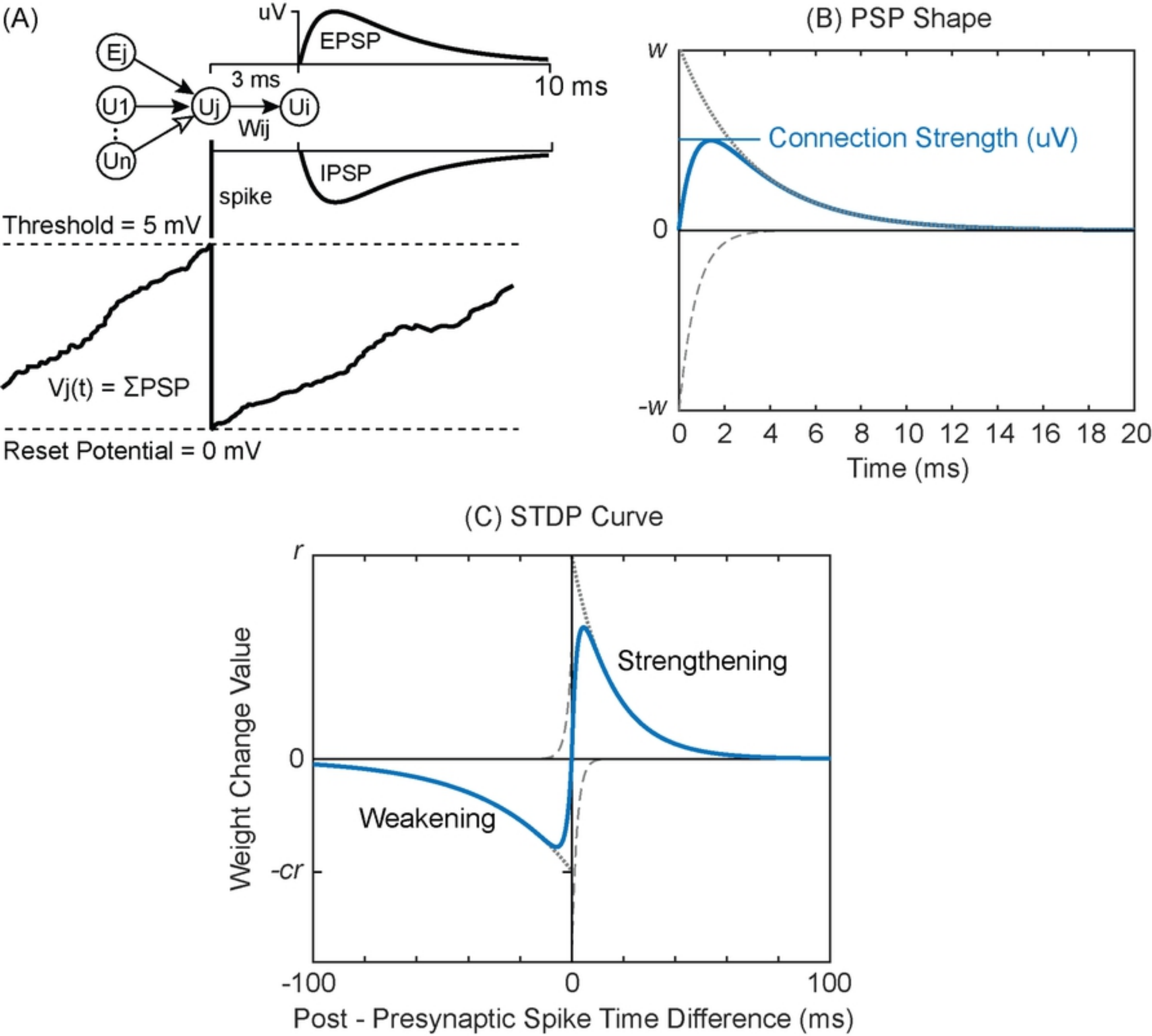
(A)
uV
EPSP
Ej
U1
Un
Uj
Ui
3 ms
10 ms
Wij
IPSP
spike
Threshold = 5 mV
Vj(t) = ΣPSP
Reset Potential = 0 mV
(B) PSP Shape
w
Connection Strength (uV)
0
-w
0 2 4 6 8 10 12 14 16 18 20
Time (ms)
(C) STDP Curve
r
Strengthening
0
Weakening
-cr
Weight Change Value
-100
0
100
Post - Presynaptic Spike Time Difference (ms)

Figure 1

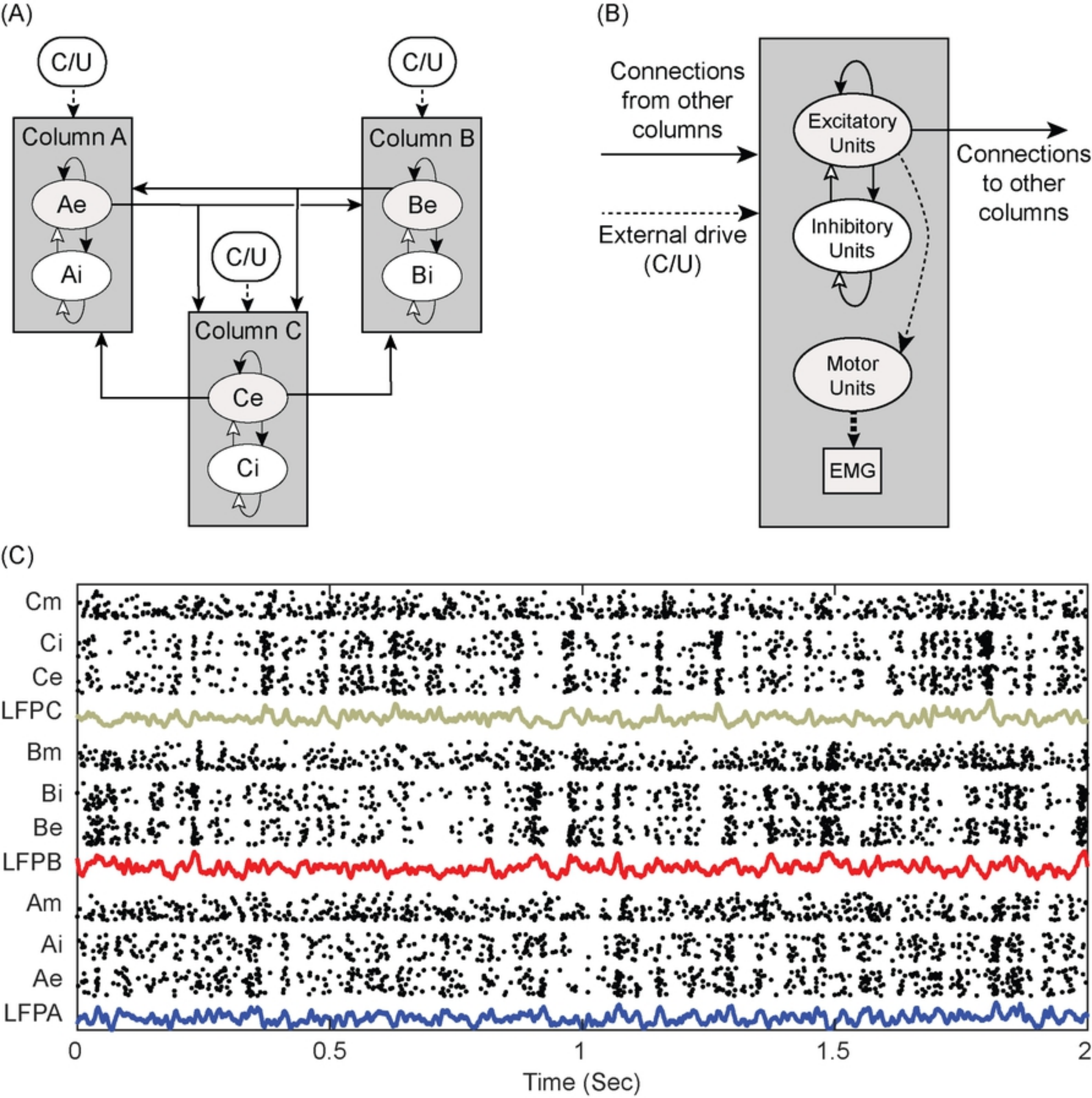
(A)
C/U
C/U
Column A
Column B
Ae
Be
Ai
Bi
C/U
Column C
Ce
Ci
(B)
Connections from other columns
External drive (C/U)
Excitatory Units
Inhibitory Units
Motor Units
EMG
Connections to other columns
(C)
Cm
Ci
Ce
LFPC
Bm
Bi
Be
LFPB
Am
Ai
Ae
LFPA
0
0.5
1
1.5
2
Time (Sec)

Figure 2

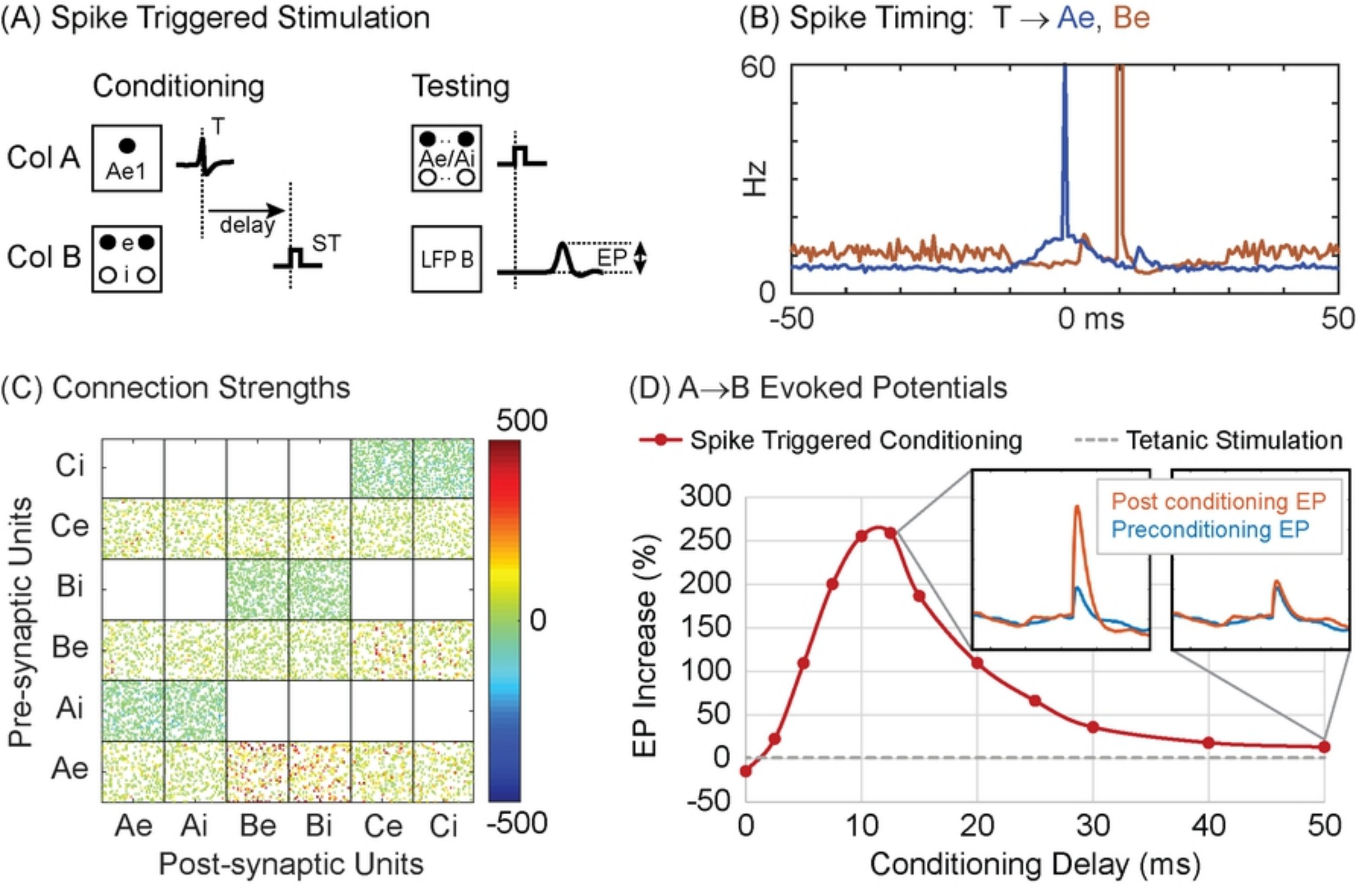
(A) Spike Triggered Stimulation
Conditioning
Testing
Col A
Ae1
T
delay
ST
Col B
e
i
Ae/Ai
LFP B
EP
(B) Spike Timing: T → Ae, Be
60
Hz
0
-50
0 ms
50
(C) Connection Strengths
500
0
-500
Ci
Ce
Bi
Be
Ai
Ae
Pre-synaptic Units
Ae Ai Be Bi Ce Ci
Post-synaptic Units
(D) A→B Evoked Potentials
Spike Triggered Conditioning
Tetanic Stimulation
Post conditioning EP
Preconditioning EP
EP Increase (%)
300
250
200
150
100
50
0
-50
0 10 20 30 40 50
Conditioning Delay (ms)

Figure 3

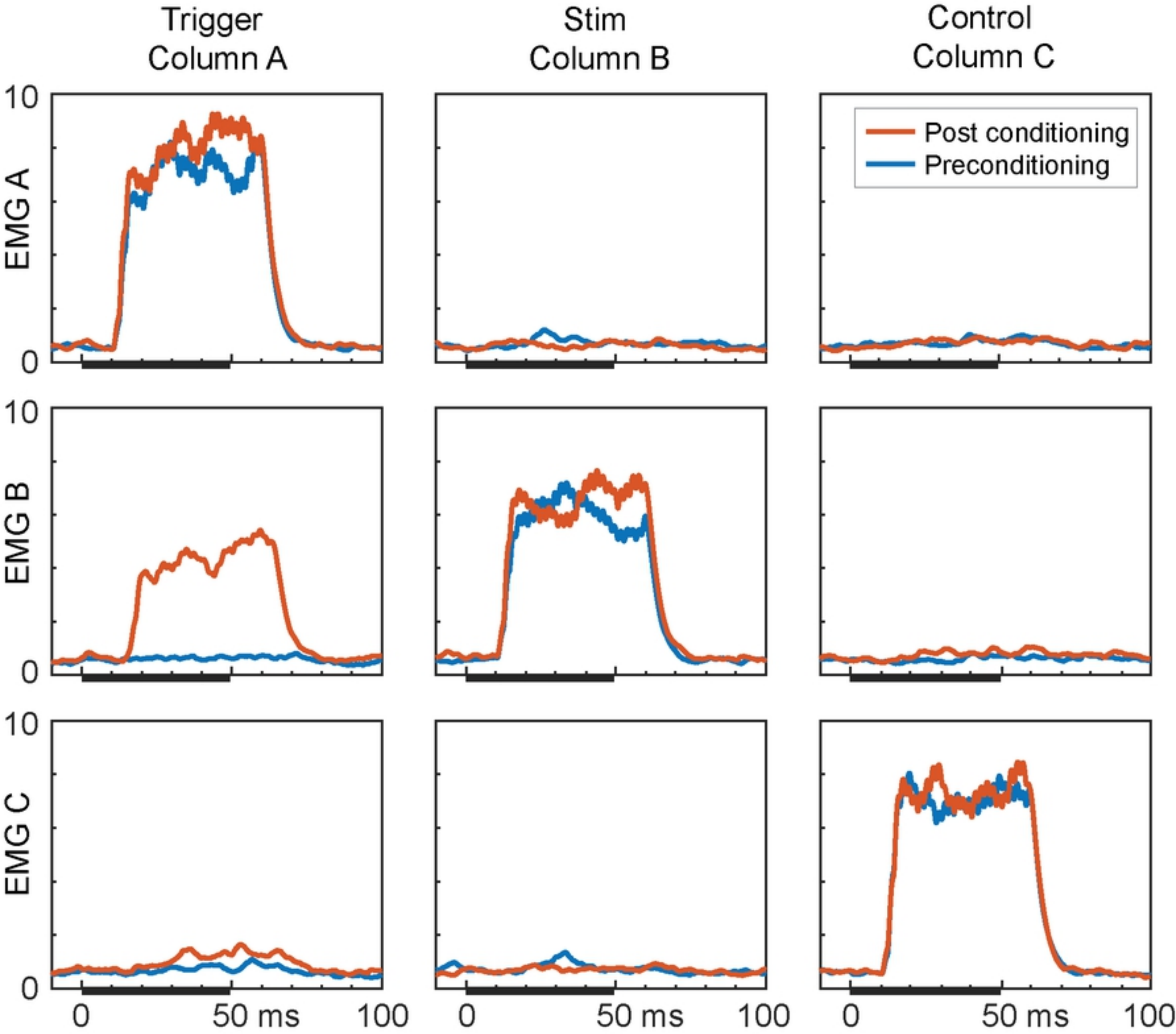
Trigger
Column A
Stim
Column B
Control
Column C
Post conditioning
Preconditioning
EMG A
EMG B
EMG C
10
0
0
50 ms
100

Figure 4

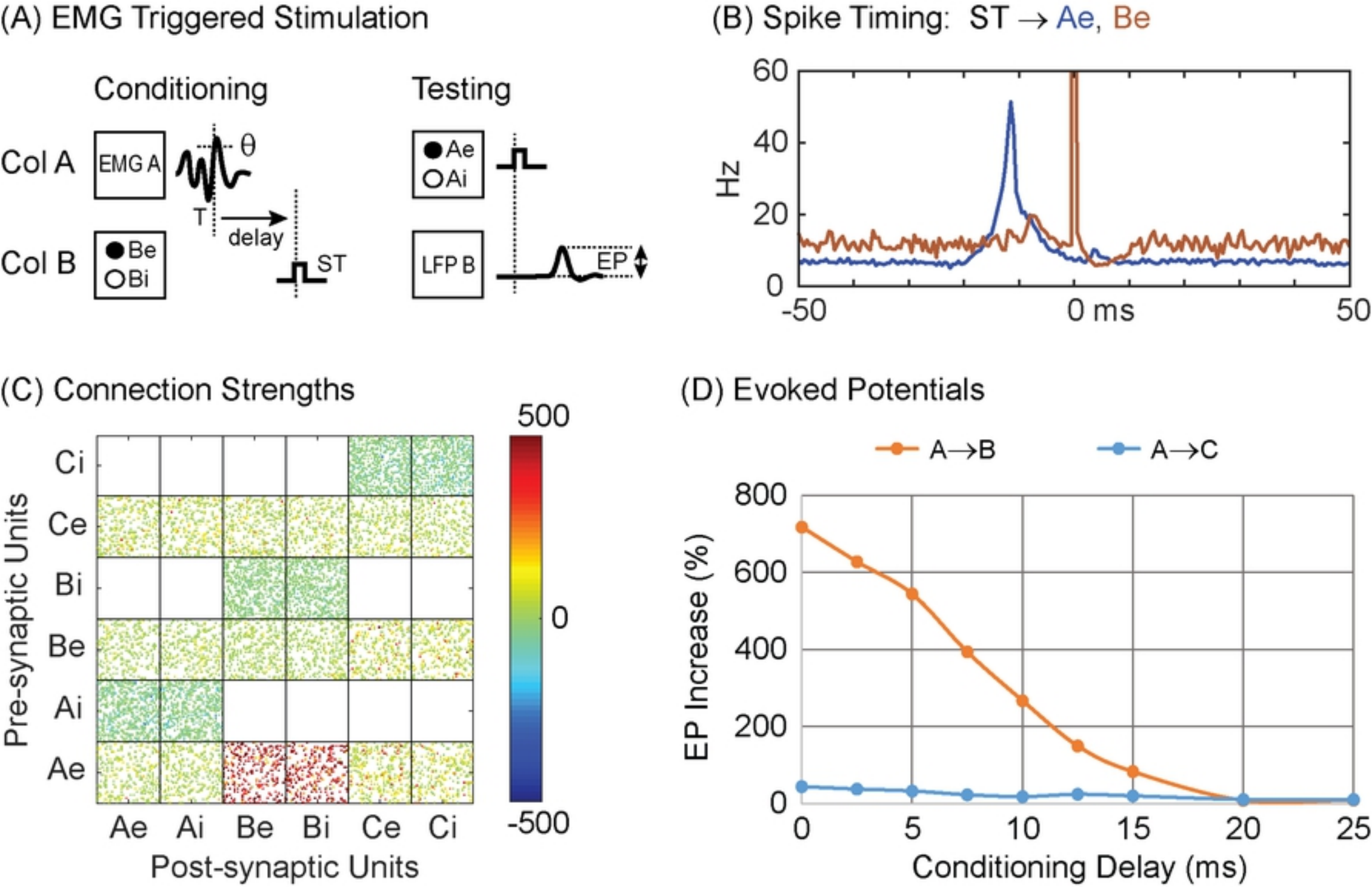
(A) EMG Triggered Stimulation
Conditioning
Testing
Col A
EMG A
θ
T
delay
Col B
Be
Bi
ST
Ae
Ai
LFP B
EP
(B) Spike Timing: ST → Ae, Be
Hz
60
40
20
0
-50
0 ms
50
(C) Connection Strengths
Pre-synaptic Units
Ci
Ce
Bi
Be
Ai
Ae
Ae Ai Be Bi Ce Ci
Post-synaptic Units
500
0
-500
(D) Evoked Potentials
A→B
A→C
EP Increase (%)
800
600
400
200
0
0 5 10 15 20 25
Conditioning Delay (ms)

Figure 5

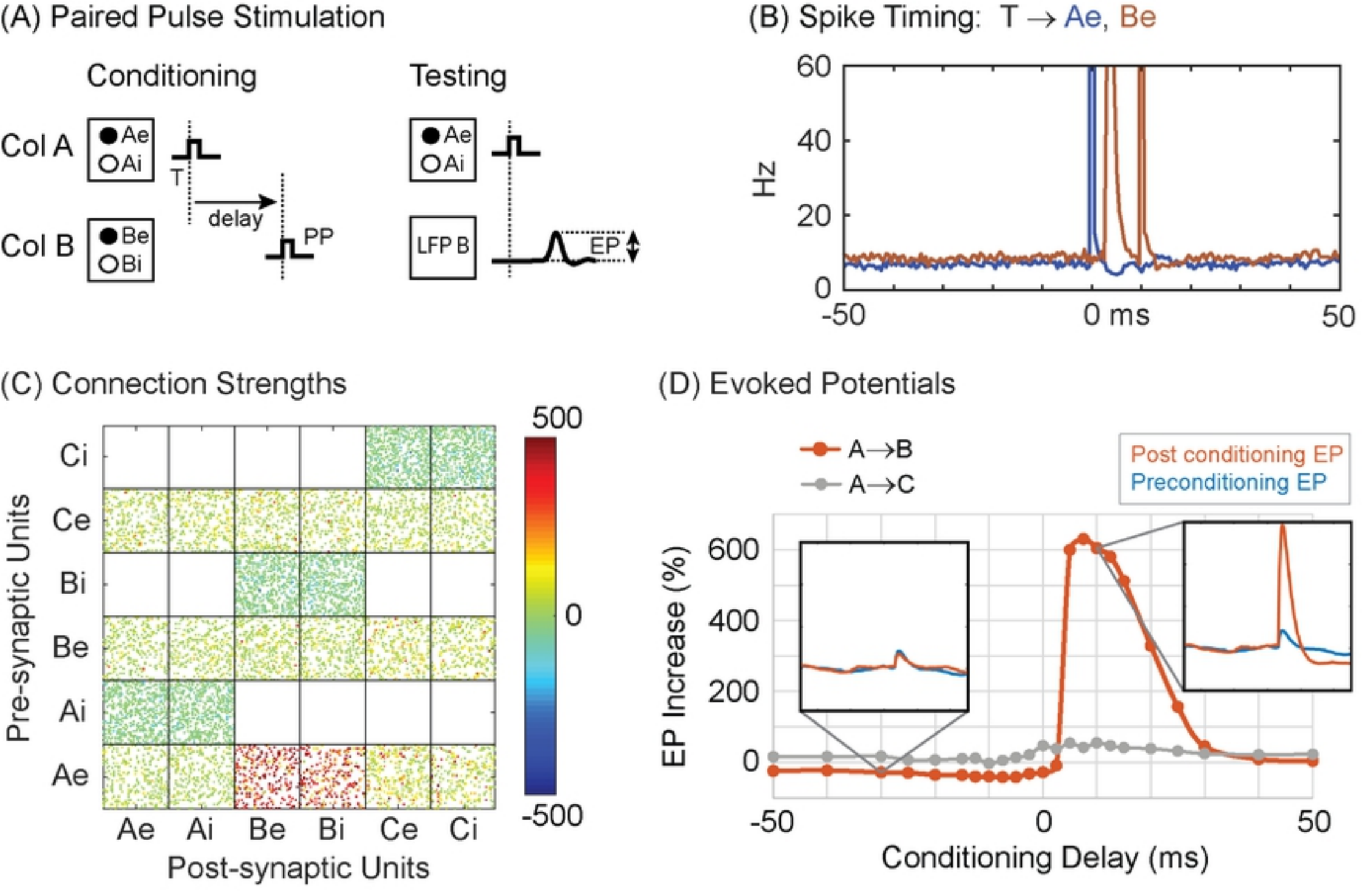
(A) Paired Pulse Stimulation
Conditioning
Testing
Col A
Ae
Ai
T
delay
Col B
Be
Bi
PP
LFP B
EP
(B) Spike Timing: T → Ae, Be
Hz
60
40
20
0
-50
0 ms
50
(C) Connection Strengths
Pre-synaptic Units
Ci
Ce
Bi
Be
Ai
Ae
Post-synaptic Units
500
0
-500
(D) Evoked Potentials
A→B
A→C
Post conditioning EP
Preconditioning EP
EP Increase (%)
600
400
200
0
-50
0
50
Conditioning Delay (ms)

Figure 6

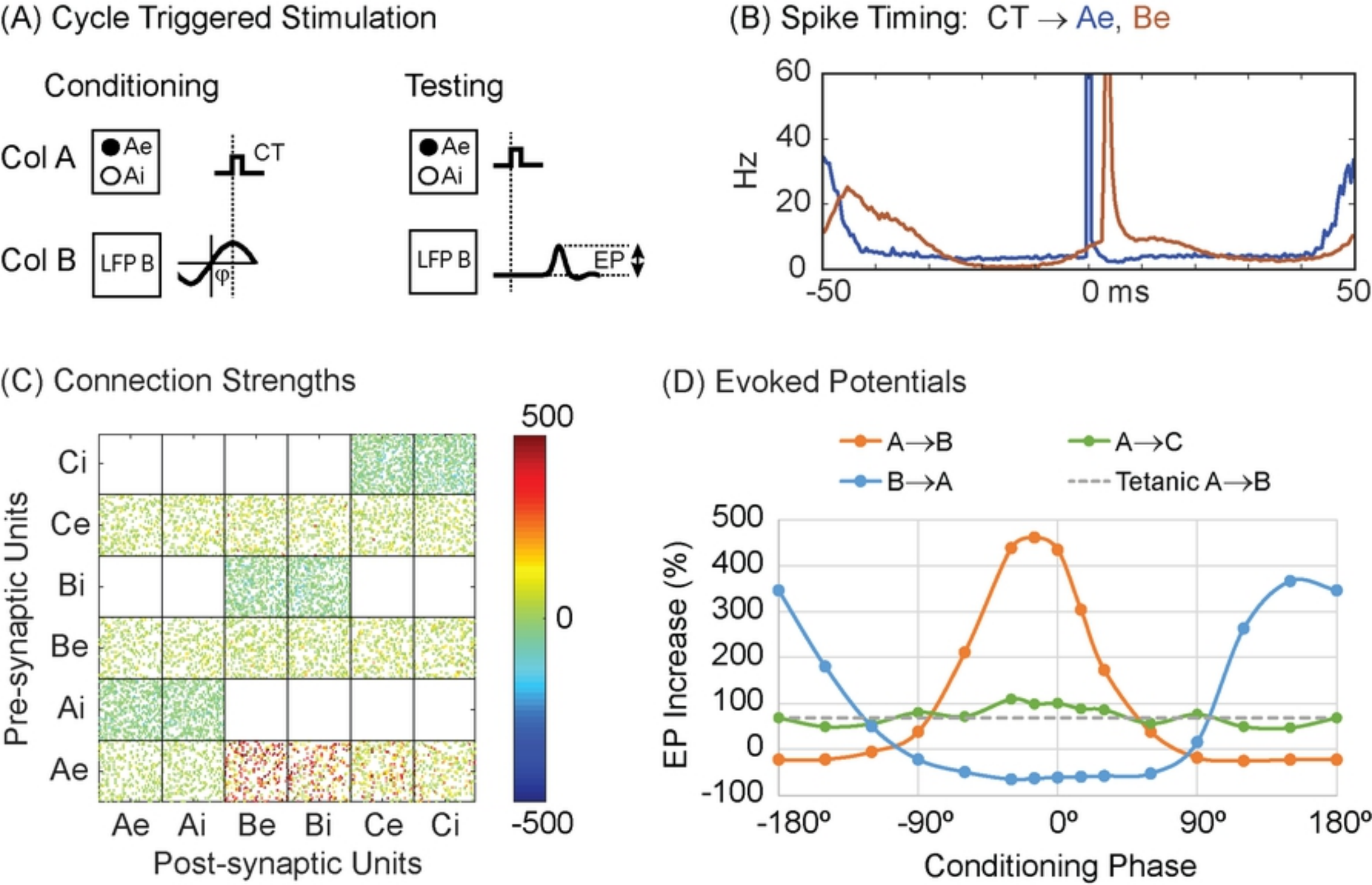
(A) Cycle Triggered Stimulation
Conditioning
Testing
Col A
Ae
Ai
CT
Col B
LFP B
φ
EP
(B) Spike Timing: CT → Ae, Be
Hz
60
40
20
0
-50
0 ms
50
(C) Connection Strengths
Pre-synaptic Units
Ci
Ce
Bi
Be
Ai
Ae
Post-synaptic Units
500
0
-500
(D) Evoked Potentials
A→B
A→C
B→A
Tetanic A→B
EP Increase (%)
500
400
300
200
100
0
-100
-180º
-90º
0º
90º
180º
Conditioning Phase

Figure 7

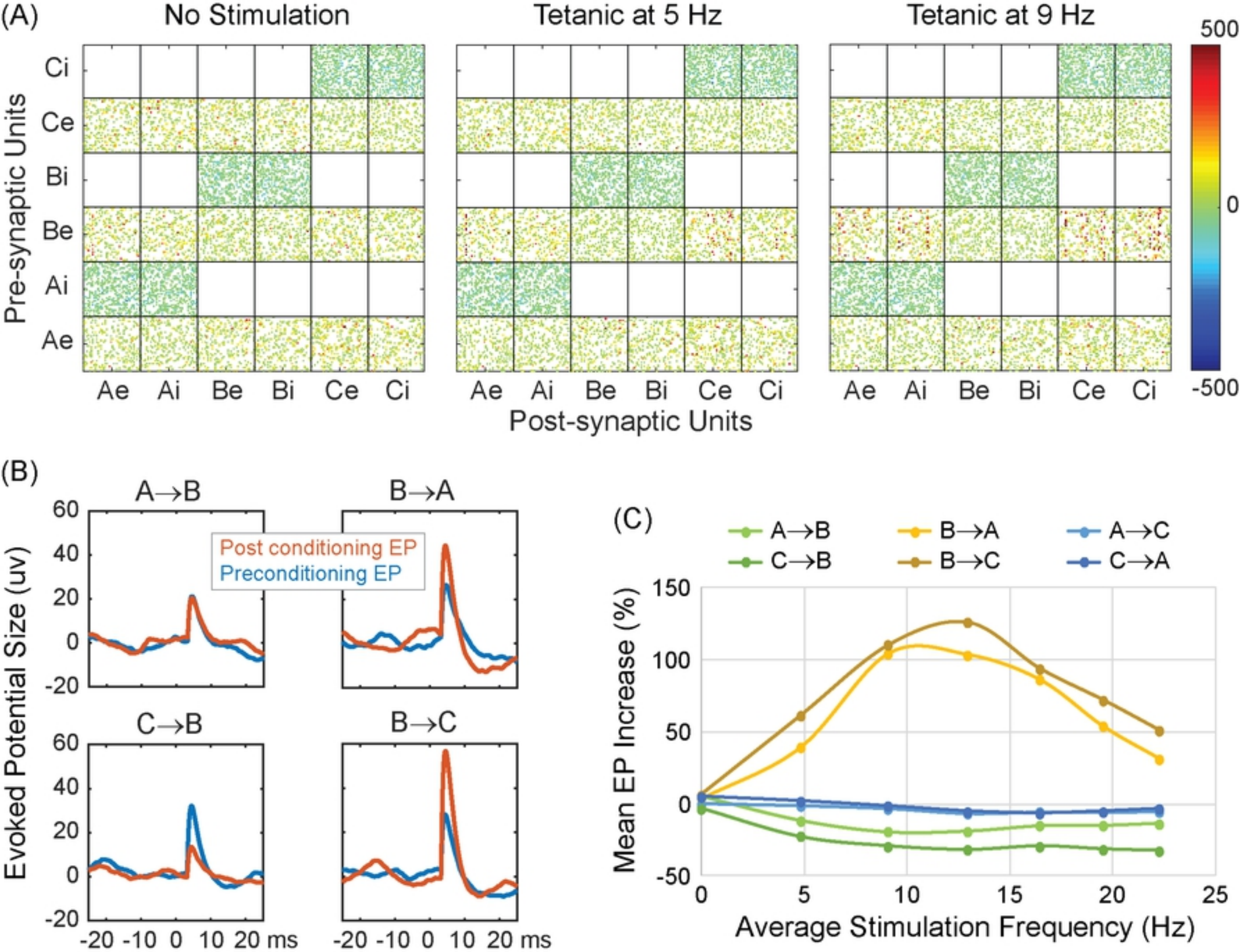
(A)
No Stimulation
Tetanic at 5 Hz
Tetanic at 9 Hz
Pre-synaptic Units
Ci
Ce
Bi
Be
Ai
Ae
Ae Ai Be Bi Ce Ci
Post-synaptic Units
500
0
-500
(B)
A→B
B→A
C→B
B→C
Post conditioning EP
Preconditioning EP
Evoked Potential Size (uv)
60
40
20
0
-20
-20 -10 0 10 20 ms
(C)
A→B
B→A
A→C
C→B
B→C
C→A
Mean EP Increase (%)
150
100
50
0
-50
0 5 10 15 20 25
Average Stimulation Frequency (Hz)

Figure 8

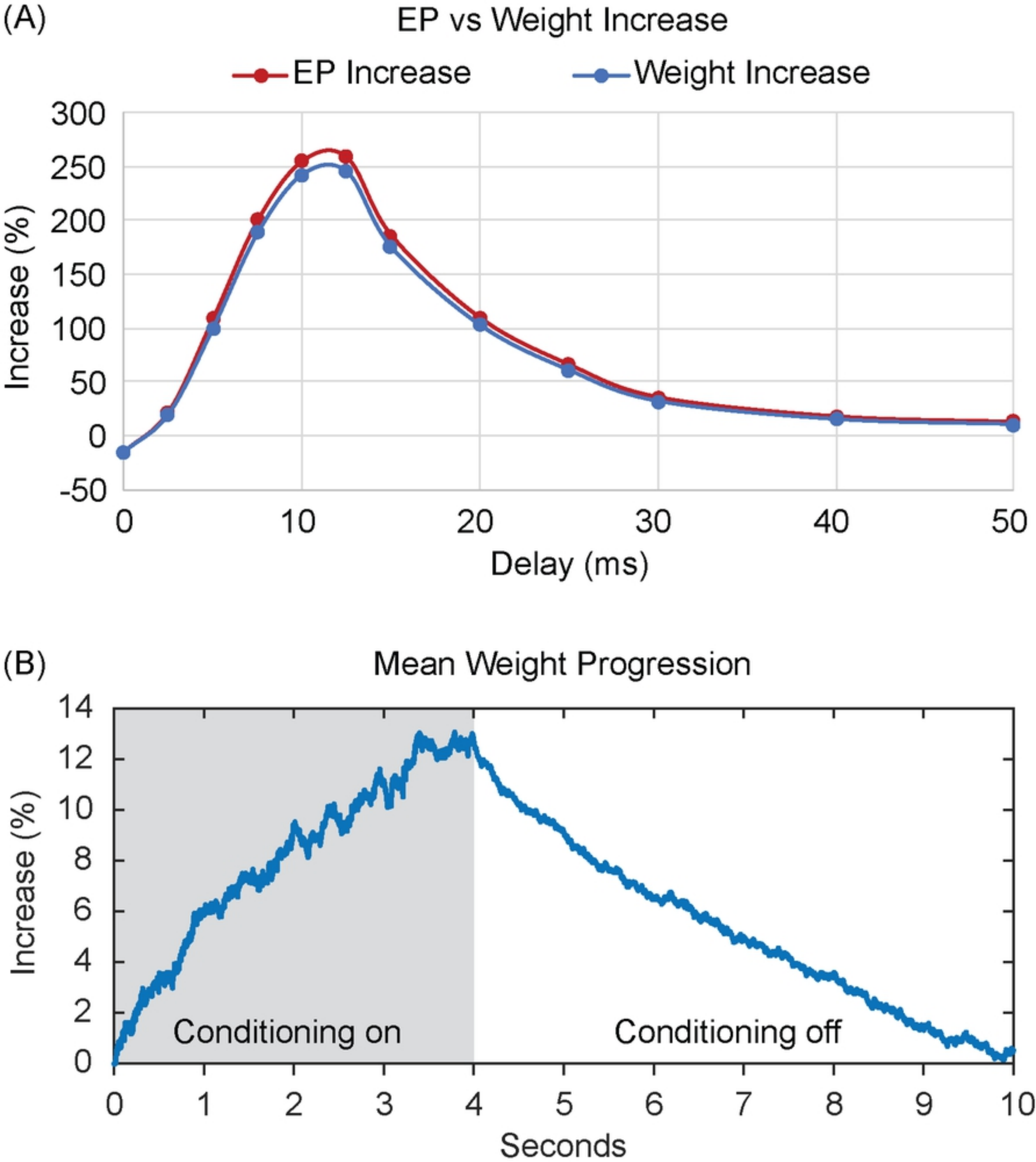
(A)
EP vs Weight Increase
EP Increase
Weight Increase
Increase (%)
300
250
200
150
100
50
0
-50
0
10
20
30
40
50
Delay (ms)
(B)
Mean Weight Progression
Increase (%)
14
12
10
8
6
4
2
0
Conditioning on
Conditioning off
0
1
2
3
4
5
6
7
8
9
10
Seconds

Figure 9

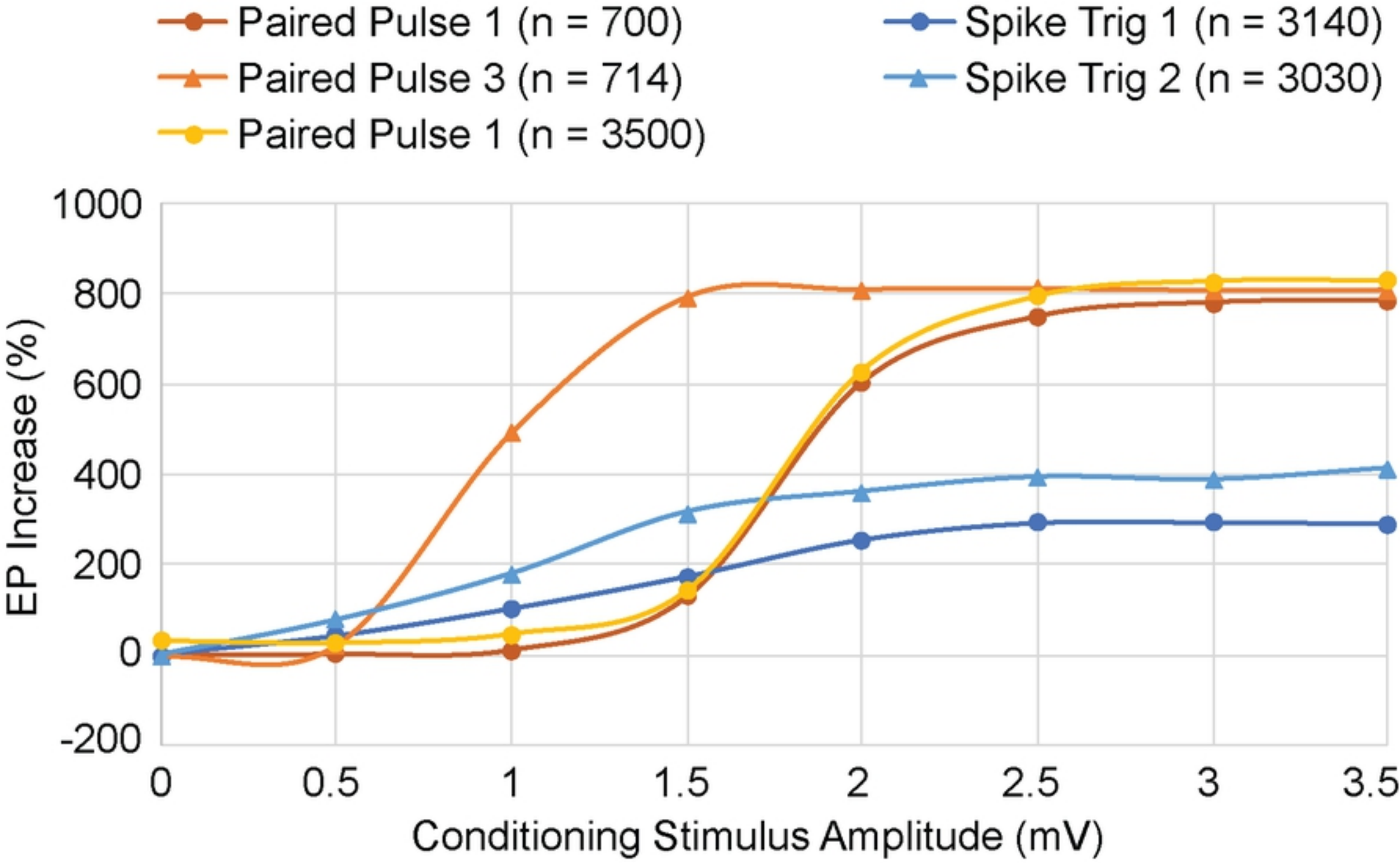
Paired Pulse 1 (n = 700)
Spike Trig 1 (n = 3140)
Paired Pulse 3 (n = 714)
Spike Trig 2 (n = 3030)
Paired Pulse 1 (n = 3500)
1000
800
600
400
200
0
-200
EP Increase (%)
0
0.5
1
1.5
2
2.5
3
3.5
Conditioning Stimulus Amplitude (mV)

Figure 10

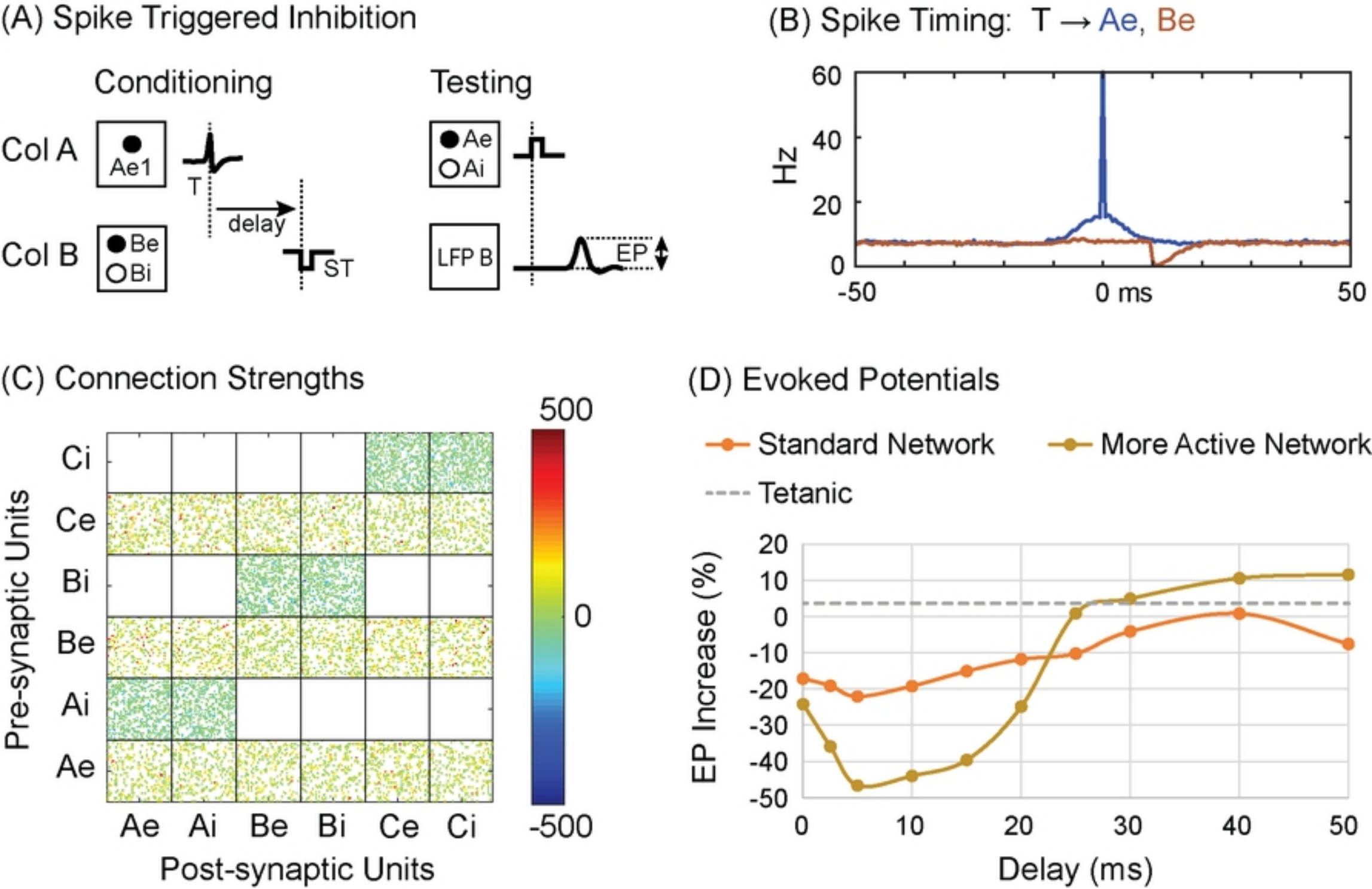
(A) Spike Triggered Inhibition
Conditioning
Testing
Col A
Ae1
T
delay
Col B
Be
Bi
ST
Ae
Ai
LFP B
EP
(B) Spike Timing: T → Ae, Be
Hz
60
40
20
0
-50
0 ms
50
(C) Connection Strengths
Pre-synaptic Units
Ci
Ce
Bi
Be
Ai
Ae
Ae Ai Be Bi Ce Ci
Post-synaptic Units
500
0
-500
(D) Evoked Potentials
Standard Network
More Active Network
Tetanic
EP Increase (%)
20
10
0
-10
-20
-30
-40
-50
0 10 20 30 40 50
Delay (ms)

Figure 11

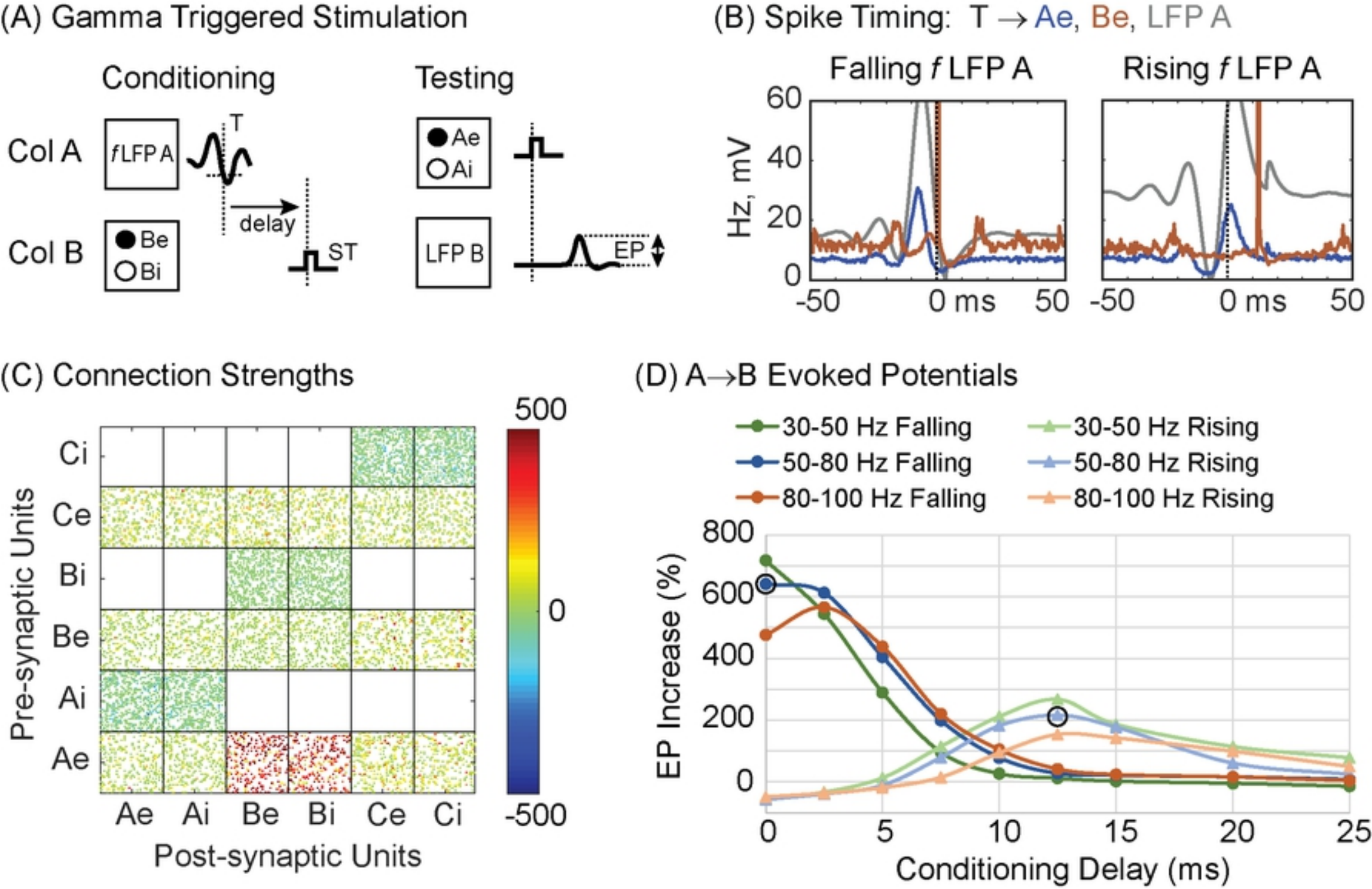
(A) Gamma Triggered Stimulation
Conditioning
Testing
Col A
fLFP A
T
Ae
Ai
delay
Col B
Be
Bi
ST
LFP B
EP
(B) Spike Timing: T → Ae, Be, LFP A
Falling f LFP A
Rising f LFP A
Hz, mV
60
40
20
0
-50
0 ms
50
(C) Connection Strengths
Pre-synaptic Units
Ci
Ce
Bi
Be
Ai
Ae
Post-synaptic Units
500
0
-500
(D) A→B Evoked Potentials
30-50 Hz Falling
30-50 Hz Rising
50-80 Hz Falling
50-80 Hz Rising
80-100 Hz Falling
80-100 Hz Rising
EP Increase (%)
800
600
400
200
0
5
10
15
20
25
Conditioning Delay (ms)

Figure 12

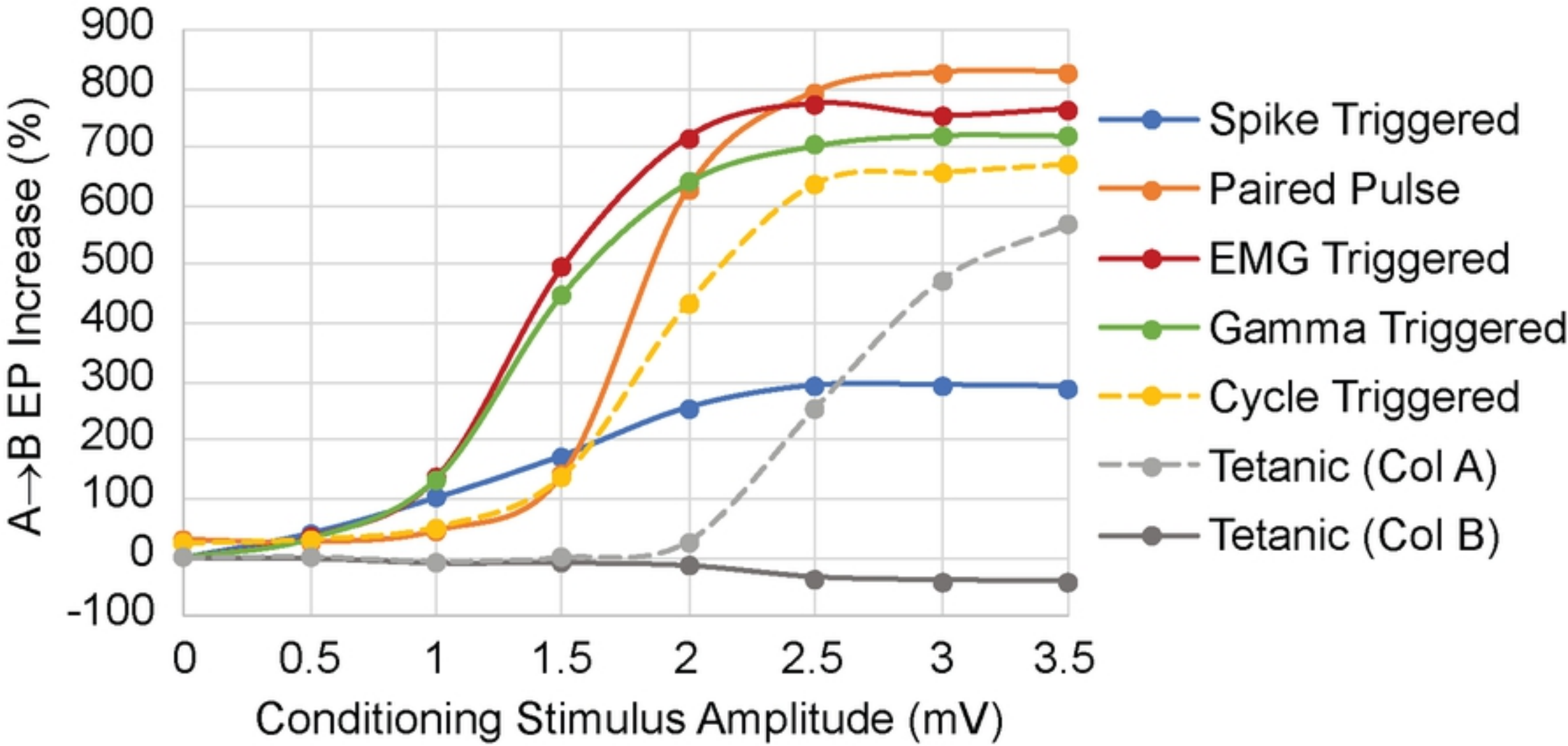
900
800
700
600
500
400
300
200
100
0
-100
A→B EP Increase (%)
0
0.5
1
1.5
2
2.5
3
3.5
Conditioning Stimulus Amplitude (mV)
Spike Triggered
Paired Pulse
EMG Triggered
Gamma Triggered
Cycle Triggered
Tetanic (Col A)
Tetanic (Col B)

Figure 13

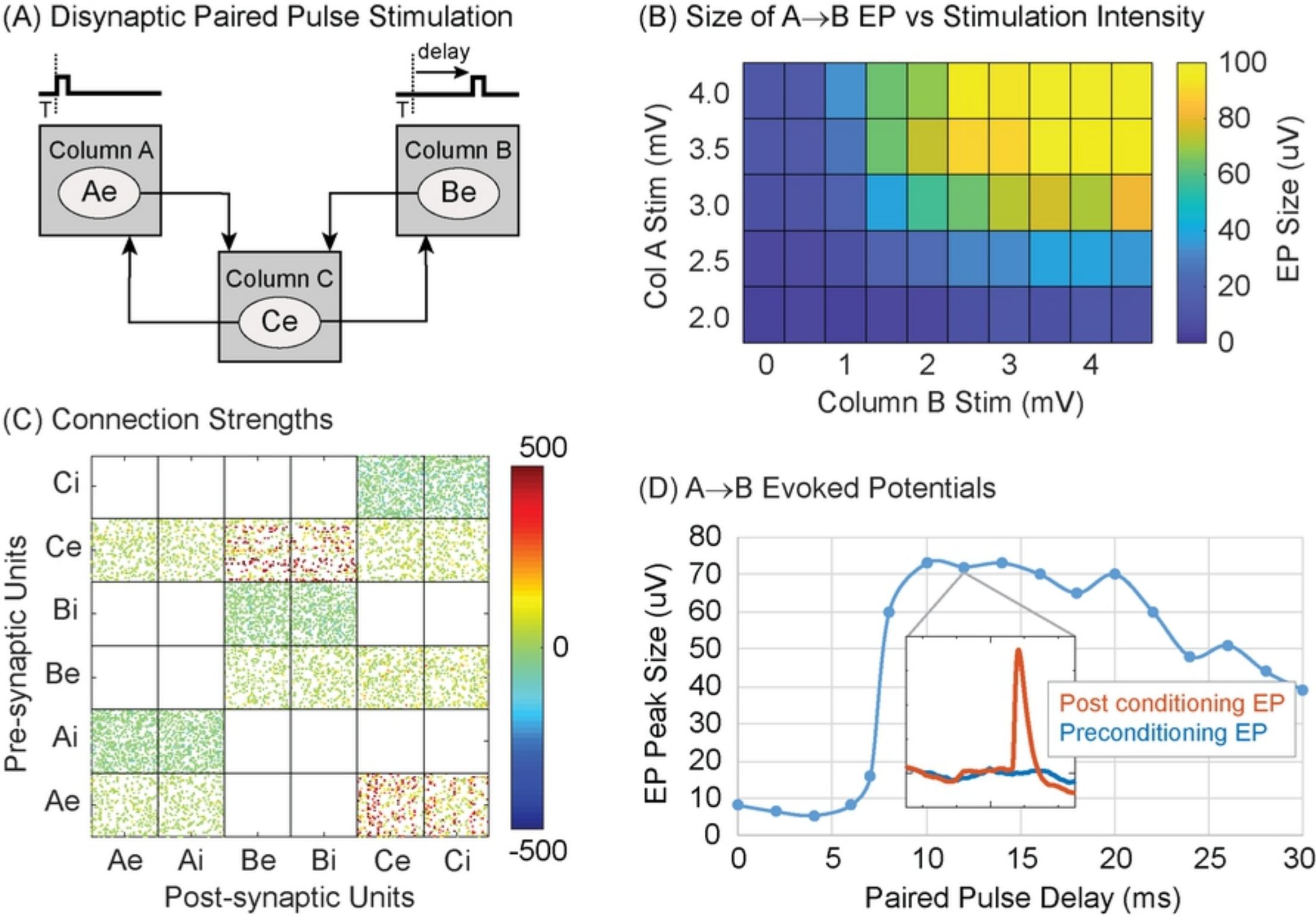
(A) Disynaptic Paired Pulse Stimulation
delay
T
T
Column A
Ae
Column B
Be
Column C
Ce
(B) Size of A→B EP vs Stimulation Intensity
Col A Stim (mV)
4.0
3.5
3.0
2.5
2.0
0
1
2
3
4
Column B Stim (mV)
100
80
60
40
20
0
EP Size (uV)
(C) Connection Strengths
Pre-synaptic Units
Ci
Ce
Bi
Be
Ai
Ae
Ae
Ai
Be
Bi
Ce
Ci
Post-synaptic Units
500
0
-500
(D) A→B Evoked Potentials
EP Peak Size (uV)
80
70
60
50
40
30
20
10
0
0
5
10
15
20
25
30
Paired Pulse Delay (ms)
Post conditioning EP
Preconditioning EP

Figure 14

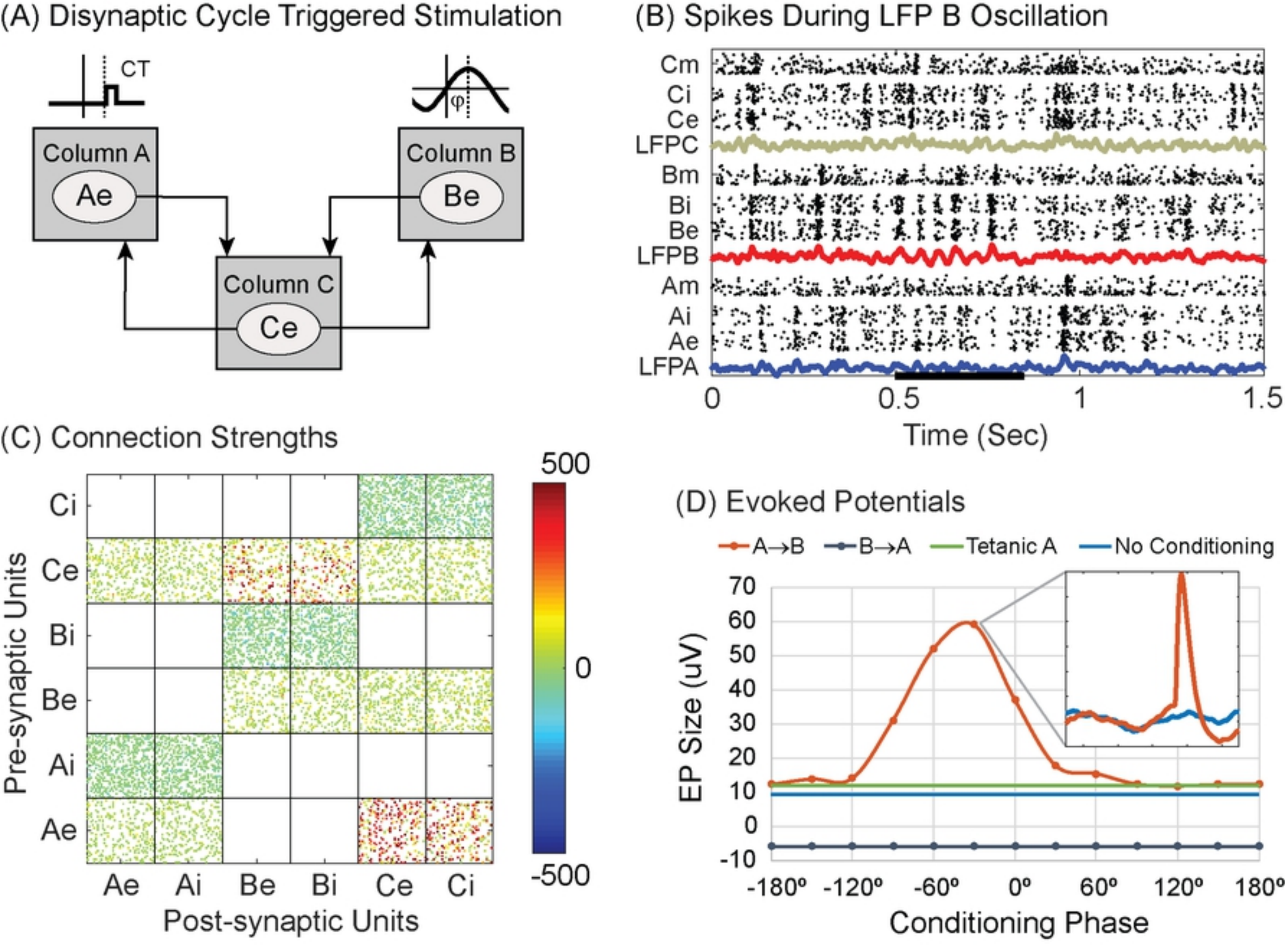
(A) Disynaptic Cycle Triggered Stimulation
CT
φ
Column A
Ae
Column B
Be
Column C
Ce
(B) Spikes During LFP B Oscillation
Cm
Ci
Ce
LFPC
Bm
Bi
Be
LFPB
Am
Ai
Ae
LFPA
0
0.5
1
1.5
Time (Sec)
(C) Connection Strengths
Ci
Ce
Bi
Be
Ai
Ae
Pre-synaptic Units
Ae
Ai
Be
Bi
Ce
Ci
Post-synaptic Units
500
0
-500
(D) Evoked Potentials
A→B
B→A
Tetanic A
No Conditioning
70
60
50
40
30
20
10
0
-10
EP Size (uV)
-180º
-120º
-60º
0º
60º
120º
180º
Conditioning Phase

Figure 15

(A) Intact Network Conditioning

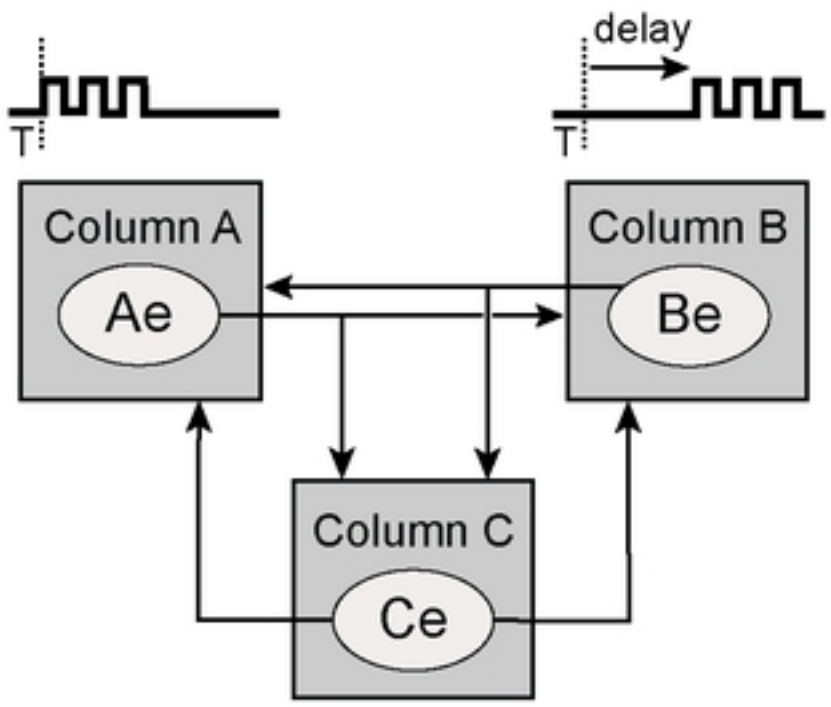

(B) Evoked Potential Testing

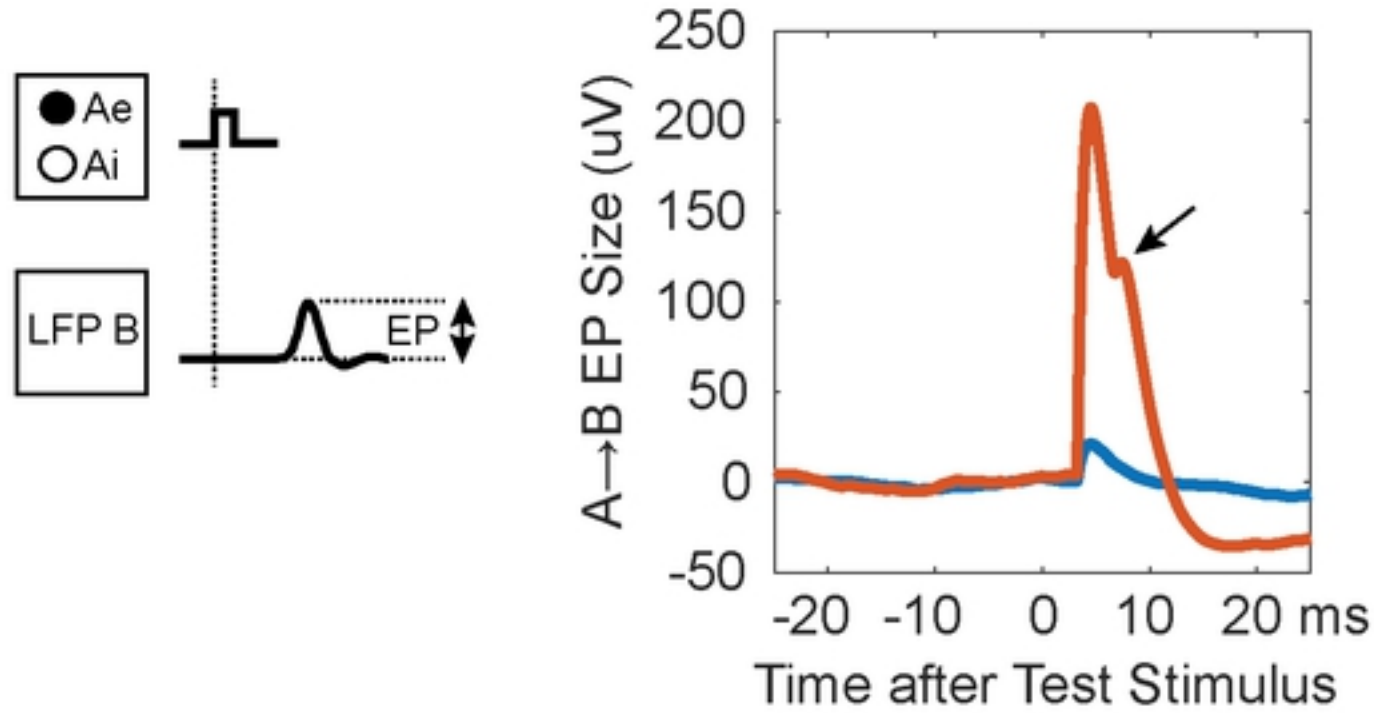

(C) Lesioned Network Conditioning

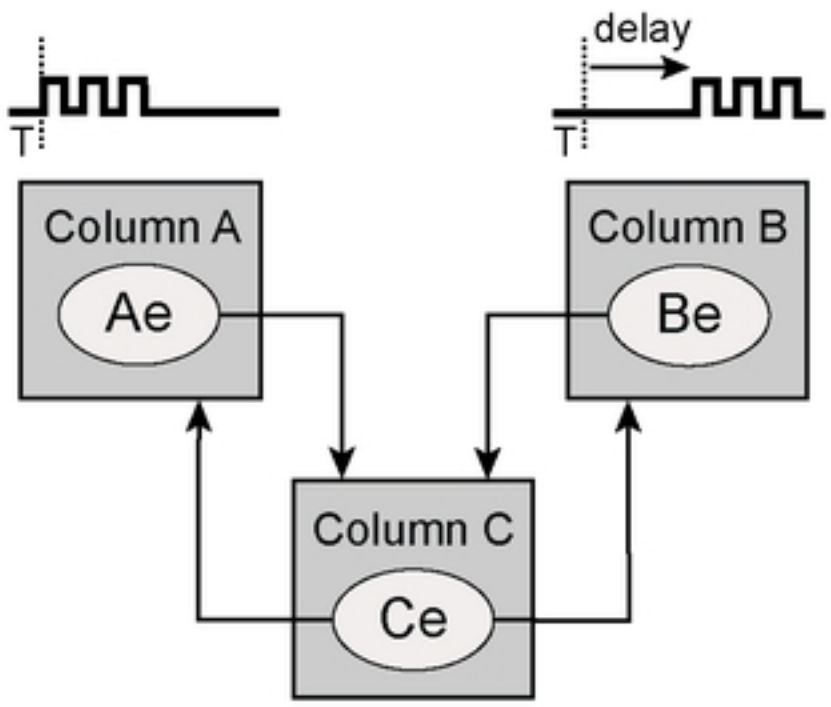

(D) Evoked Potential Testing

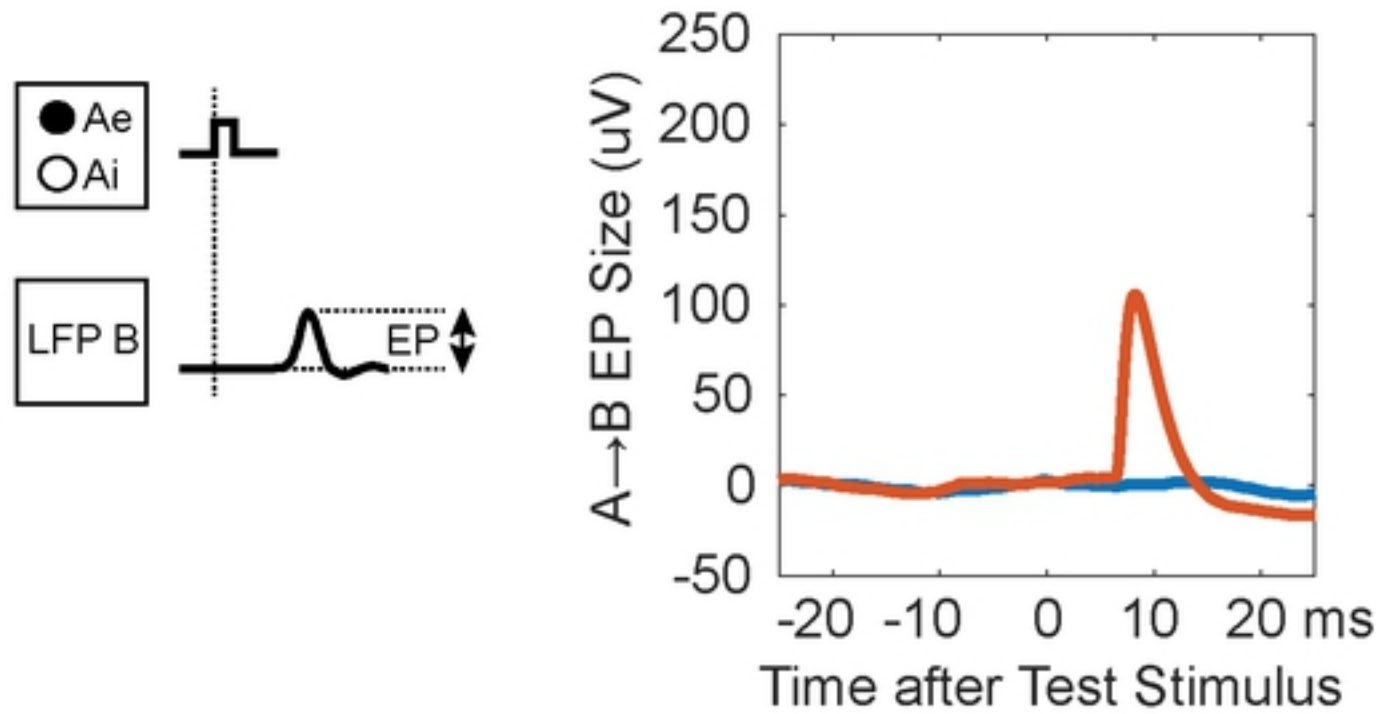

(E) Intact vs Lesioned Network for 10 Random Initial Conditions

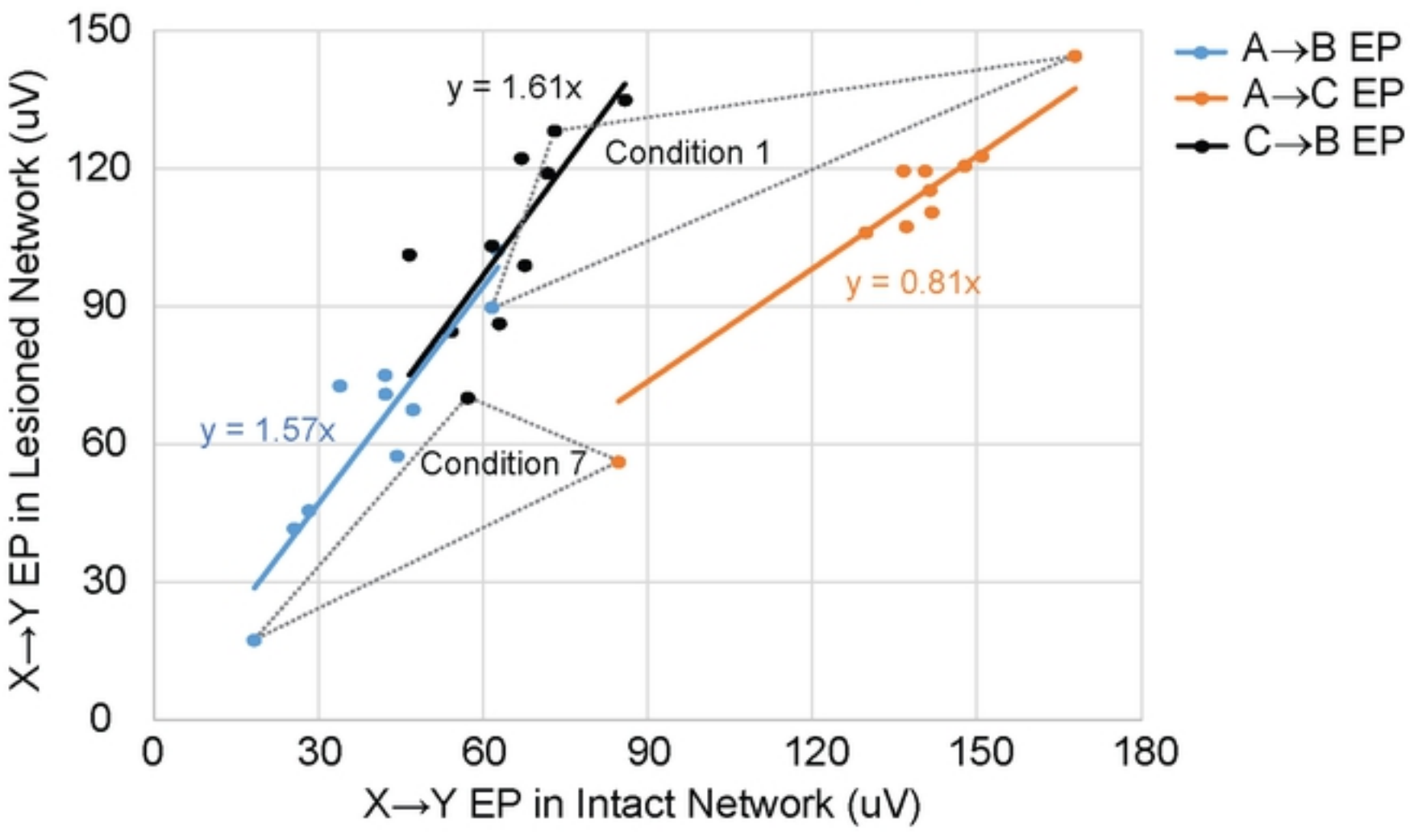

Figure